Master's thesis

NTNU
Norwegian University of Science and Technology
Faculty of Information Technology and Electrical Engineering
Department of Electric Power Engineering

Kyrre Kirkbakk Fjær

Analysis of Dynamic Pricing to utilise Spatial Flexibility in Heavy-Duty Electric Vehicle Charging Demand

Master's thesis in Energy and Environmental Engineering
Supervisor: Magnus Korpås (NTNU)
Co-supervisor: Bendik Nybakk Torsæter (SINTEF Energi AS) and Michele Garau (SINTEF Energi AS)

June 2021

NTNU
Norwegian University of Science and Technology

Kyrre Kirkbakk Fjær

Analysis of Dynamic Pricing to utilise Spatial Flexibility in Heavy-Duty Electric Vehicle Charging Demand

Master's thesis in Energy and Environmental Engineering
Supervisor: Magnus Korpås (NTNU)
Co-supervisor: Bendik Nybakk Torsæter (SINTEF Energi AS) and Michele Garau (SINTEF Energi AS)
June 2021

Norwegian University of Science and Technology
Faculty of Information Technology and Electrical Engineering
Department of Electric Power Engineering

NTNU
Norwegian University of
Science and Technology

Abstract

The upcoming heavy-duty electric vehicles (HDEVs) are expected to have a charging power between 400 kW and 1600 kW. A transition to HDEVs can cause challenges to the power grid to deliver the charging power needed. Typically, these challenges are coped with by upgrading the components in the power grid, which may be very costly in many areas. Therefore, it is necessary to investigate if there are other solutions to handle the new load demands. A possible solution is utilising demand response and dynamic pricing. By changing the charging price at a high-power charging station dynamically, based on the grid conditions, it is possible to incentivise the drivers to charge at other locations where the grid conditions are better. Thus, available flexibility in the power grid is utilised to increase stability.

This thesis aims to investigate the impact of dynamic pricing to distribute the load from HDEVs in a more favourable manner between two high-power charging stations. A new method for dynamic pricing of high-power charging stations by utilising the nodal prices from optimal power flow calculations is proposed. To investigate the proposed method, an agent-based model used to simulate traffic and charging behaviour is extended to include HDEVs and the new proposed dynamic pricing scheme. The dynamic pricing scheme is then compared to two different pricing schemes, a fixed pricing scheme and a dynamic pricing scheme that consider the voltage levels in the system.

From the case studies, it is evident that the dynamic pricing schemes are able to distribute the HDEVs more favourably and thus move load from a weak bus to a stronger bus. In one topology, the daily minimum voltage magnitudes at the weakest bus have, on average, been raised with 0.005 p.u. and 0.004 p.u. with OPF and voltage based dynamic pricing, respectively. While it in certain time steps have increased with as much as 0.02 p.u. for both pricing schemes. The voltage-based dynamic pricing scheme has decreased the losses from 4.75 % to 4.65 %, while the OPF based pricing scheme has reduced the losses further to 4.55 %. The results have shown a positive impact from both dynamic pricing scheme, where the OPF based tend to outperform the voltage based dynamic pricing scheme.

The two dynamic pricing schemes are strongly dependent on the power system topology and traffic environment. In an additionally investigated power system topology, an unwanted effect is observed from using the two dynamic pricing schemes. At some time steps, the voltage drops have been amplified, thus creating worse gird conditions. This is due to the shortcomings in both dynamic pricing schemes as they are approaches that utilise previously measured load conditions and do not predict the upcoming loads. Thus, the method is poorly adapted to handle significant load changes in the next time steps.

Sammendrag

De kommende elektriske lastebilene for tungtransport forventes å kreve ladeeffekter mellom 400 kW og 1600 kW. En overgang til elektriske lastebiler kan dermed føre til utfordringer for strømnettet til å levere ladekraften som trengs. Vanligvis håndteres disse utfordringene ved å oppgradere komponentene i strømnettet, noe som kan være svært kostbart mange steder. Derfor er det nødvendig å undersøke om det finnes andre løsninger for å håndtere disse nye og større ladeprofilene. En mulig løsning er å endre etterspørselen på ulike ladestasjoner ved å bruke dynamisk prising. Ved å endre ladeprisen på en ladestasjon, basert på nettforholdene, er det mulig å motivere sjåførene til å lade på andre stasjoner som er plassert steder der nettforholdene er bedre. Noe som muliggjør utnyttelse av fleksibiliteten i strømnettet for å bedre nettforholdene.

Denne oppgaven undersøker virkningen av dynamisk prising til å fordele ladebelastningen fra elektriske lastebiler på en mer gunstig måte mellom to ladestasjoner. Det foreslås en ny metode for dynamisk prising av ladestasjoner ved å benytte nodeprisene fra beregninger av optimal lastflyt (OPF). For å teste ut denne metoden utvides en agentbasert modell, som brukes til å simulere trafikk- og ladeadferd, til å inkludere elektriske lastebiler og den nye dynamiske prisordningen. Den dynamiske prisordningen sammenlignes deretter med to forskjellige metoder i en casestudie, der prsien holdes konstant i et scenario og endres dynamisk basert på spenningsnivåer i et annet.

Fra studiene er det tydelig at de dynamiske prisordningene er i stand til å distribuere elektriske lastebiler på en mer gunstig måte og dermed flytte belastning fra en svak node til en sterk node. I det ene strømnettet er den daglige minimumsverdien på spenning i den svakeste noden i gjennomsnitt hevet med 0,005 p.u. og 0,004 p.u., med henholdsvis OPF og spenningsbasert dynamisk prising. På enkelte tidspunkt har spenningen økt med 0,02 p.u. for begge de dynamiske prisordningene. Den spenningsbaserte dynamiske prisordningen har redusert tapene fra 4,75% til 4,65%, mens den OPF-baserte prisordningen har redusert tapene ytterligere til 4,55%. Resultatene har vist en positiv innvirkning fra begge de to dynamiske prisordningene, der den OPF-baserte prisordningen oftere skaper gunstigst nettforhold av de to.

Det er tydelig fra studiene at de to dynamiske prisordningene er sterkt avhengig av strømnettets topologi. I en anne topologi av strømnettet blir det observert en uønsket effekt av å bruke de to dynamiske prisplanene. På enkelte tidspunkt blir spenningsfallene forsterket, og skaper dermed dårligere nettforhold. Dette er på grunn av begrensninger i begge de dynamiske prisordningene. Begge metodene lager prissignaler som benytter seg av målt data fra tidligere tidspunkt. Dette fører til at prissignalene ikke tar hensyn til hvordan tilstanden i strømnettet kommer til å være i de fremtidige tidsstegene den kalkulerte prisen er gjeldende. Dermed er metodene dårlig tilpasset for å håndtere store endringer i lasten fra en periode til den neste.

Preface

This master's thesis is submitted as the final work for my Master of Science degree in Energy and Environmental Engineering at the Norwegian University of Science and Technology. The thesis was completed in the spring semester of 2021 and continues on the same topic as in the project thesis, written during autumn 2020. In parallel with the work on this thesis, I have been given the great opportunity of writing my first scientific paper. The paper is based on the simulations conducted in my project thesis and is added in the appendix B.

This work is conducted in collaboration with the FuChar project, and I gratefully acknowledge the FuChar project consortium for contributing to this work with their knowledge and experience. FuChar is a KPN project funded by The Research Council of Norway and industry partners (grant no. 295133/E20). The author would also like to thank Elvia for their contribution of data.

I want to thank my supervisor, Professor Magnus Korpås, for your guidance and motivation throughout the last year. It has always been great to discuss the work and other things at your office or in digital meetings. I would also like to thank my co-supervisor, Bendik Nybakk Torsæter, at SINTEF Energy Research, for your valuable help and guidance with both the master's thesis and the writing of the scientific paper. Also, I want to give a big thanks to co-supervisor Michele Garau at SINTEF Energy Research for sharing your knowledge and model from previous work, in addition to helping me understand the concept of agent-based modelling. I would also thank Venkatachalam Lakshmanan at SINTEF Energy Research for your guidance on the scientific paper and encouraging chats throughout the semester. At last, I want to thank friends and family for being fantastic persons in my life.

Trondheim, June 2021

Kyrre Kirkbakk Fjær

Contents

List of Figures

List of Tables

List of Abbreviations

ACOPF AC Optimal Power Flow

DCOPF DC Optimal Power Flow

DSO Distribution system operator

EV Electric Vehicle

HDEV Heavy-Duty Electric Vehicle

HDV Heavy-duty Vehicle

HPCS High-power charging station

LDV Light-Duty Vehicle

NVE The Norwegian Water Resources and Energy Directorate

OPF Optimal Power Flow

1 Introduction

1.1 Motivation

New energy technologies must be included to cope with the 2° Celsius limit in the Paris agreement. The transport sector is responsible for 20 % of the CO_2 emissions worldwide. Road transport is the most significant contributor, with 75 % of the emissions from the sector, [1]. By changing from classical internal combustion engines (ICE) to fuel-cell or battery-electric vehicles (BEVs), there is significant potential in reducing the emissions. However, the transition from ICE to BEVs creates a greater demand for electricity from the power grid. The increased share of BEVs will increase the electricity demand from the use of high-power charging stations (HPCS) that allows charging at high power rates. Today's electric vehicles (EVs[1]) are already demanding charging powers in the range of 150-350 kW, while it is in the future anticipated heavy-duty electric vehicles (HDEVs) that introduces charging power demands in the range of 400-1600 kW [1]–[3]. Thus, it is clear that the power grid has major challenges ahead. Some potential challenges that may occur if no action is taken are, e.g. high peak to average demand ratio and overloading of power system components such as substations and transmission lines. Typically, these issues are coped with by upgrading the components in the power grid, which may be very costly in many areas. Therefore, it is necessary to investigate other possible solutions to handle the new load demands and patterns.

One potential solution is to utilise the flexibility in today's grid and customer behaviour through dynamic pricing of electricity. Dynamic pricing is the concept where the distribution system operator (DSO) or the operator of an HPCS dynamically updates the price the customer must pay. By dynamically change the prices, it is possible to respond to any changes in the operating conditions of the power system. In this way, it is possible to increase the price at the HPCS when, e.g. the market prices increase, the voltage levels decreases or when the transfer capacity is threatened. The introduction of dynamic pricing may thus increase the grid stability, reduce the operating cost of HPCS and increase customer satisfaction.

1.2 Problem description

The introduction of HDEVs and corresponding HPCS introduces loads that have a significant impact on the grid conditions. This thesis aims to investigate the impact of dynamic pricing to distribute the load from HDEVs in a more favourable manner at two HPCS. The main objective is to develop a new dynamic pricing method that utilises the nodal prices calculated from an optimal power flow (OPF) to generate price signals. Secondly, extend an agent-based model, used to simulate electric vehicle (EV) charging behaviour, to include new functionalities. These are furthermost the inclusion of HDEVs and the new proposed dynamic pricing scheme. The extended model will be used in case studies to investigate the impact of the new dynamic pricing scheme. The performance will be compared to a fixed and a second dynamic pricing scheme. In addition, an additional method of evaluating which HPCS is the cheapest will be added and briefly demonstrated.

[1]The abbreviation EV is in this thesis used in the context of a electric car.

1.3 Limitations

Several assumptions and limitations have been made due to unavailable data and to simplify the study.

- To simplify the model, reactive power and power harmonics are not taken into account.
- It is assumed that the charging power is kept fixed for the whole charging session. In reality, the charging power will be reduced when the state-of-charge is reaching higher values.
- It is assumed that the expected SOC for each vehicle is distributed from the same uniform distribution throughout the whole day. In reality, the expected SOC will vary with the time of the day, but an extensive study needs to be conducted in order to define this.
- It is assumed that the vehicles do not have an upper threshold of willingness to pay. Thus, the vehicles will charge independently of how high the cheapest charging price is.
- Queuing is not taken into account. Only a maximum number of operating sockets at a time. Thus, the vehicles will drive past the area if no HPCS are available.
- Line congestion is not a part of the scope. Thus, the power system is designed accordingly.

1.4 Outline

The master's thesis is structured as followed:

- Section 2, *Background and literature review*, aims to give the necessary background information about the topic. In addition, it provides a presentation of relevant work in the literature.
- Section 3, *Theory*, gives an introduction to power flow analysis, optimal power flow calculations and an introduction to agent-based modelling.
- Section 4, *Methodology*, presents the proposed dynamic pricing method, a description of the used model and the extensions of this model.
- Section 5, *System description and cases*, describes the system and the case studies that will be investigated.
- Section 6, *Results*, presents the results from the case studies. The different cases are compared and analysed.
- Section 7, *Discussion*, discuss the main findings from the results, how to improve the proposed method and challenges to implement dynamic pricing in reality.
- Section 8, *Conclusion*, summarise and concludes the main findings.
- Section 9, *Further work*, presents suggestions for further work on the topic.

2 Background and literature review

In this section, necessary background info about the topic is given. Some parts are reused from the project thesis to give a brief status about HDEVs, charging infrastructure and the grid impact from electric transport. Background on demand response and relevant work on load modelling, grid impact analysis and dynamic pricing of EV charging is presented.

2.1 Status of HDEVs

2.1.1 Policy impact

In recent years it has been great incentives for a transition to electric vehicles in the road passenger segment, resulting in a record-high market share of 2.6% of new cars sold in 2019 [1]. However, within the road freight segment, there has not been any considerable electrical transition so far.

One of the main reasons is that the policies for heavy-duty vehicles (HDVs) are lagging cars. In 2016 nearly 85% of light-duty vehicles (LDVs) were sold in markets with fuel economy and CO_2 standards, with the same number to be 50% for HDVs. However, the momentum for policies is growing and is in 2019 nearly 70%. Some new notable policies have been introduced in India, Europe, and China. India introduced new fuel economy standards in 2018, causing policy coverage worldwide to be over 50% for the first time [4]. In July 2019, the European Union applied a new regulation that mandates the average specific CO_2 emissions to be reduced by 15% by 2025 and 30% by 2030 compared to the reference period, July 2019 to June 2020 [5]. China's Phase III Standards have raised the efficiencies of the new buses and trucks. This standard has a significant impact as China is the largest market for HDVs [4].

2.1.2 Global HDEV sales

The sales of HDEVs have historically been low, with less than 300 units sold annually worldwide until 2015. However, in 2015 there was a massive increase in sales, and almost 6000 units were sold, mainly in China. This increase was due to the government extended subsidies by eliminating the previously upper weight limits. In addition, improvements in battery technology, cost reduction, and expanding model range contributed to this increase. After that, the sales decreased in the next few years until a new jump in 2019, when it was the first time with over 6000 units sold. Nevertheless, China is still the largest market, with 6112 units sold in 2019 [1].

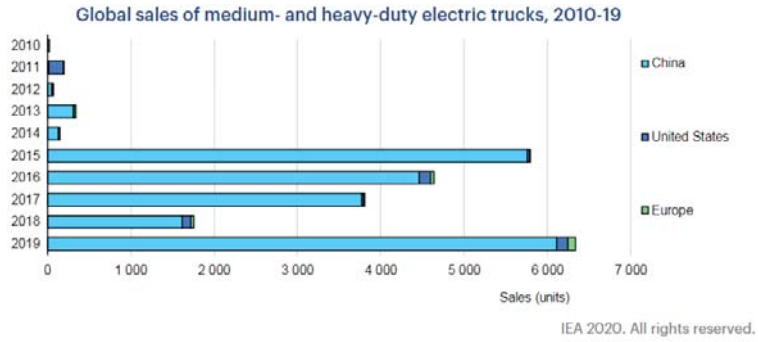

Figure 1: HDEV sales worldwide 2010-2019.

2.1.3 Charging infrastructure for HDEVs

Due to other attributes for HDEVs compared to EVs, new and larger charging stations are needed. Most new EVs have batteries in the range of 50-120 kWh and charging power of 150-350 kW. Compared to the projected sizes for HDEVs, there is a tremendous difference. The upcoming HDEVs expect to have battery sizes of 200-1000 kWh and charging power between 450-1600 kW [2], [3]. CHAdeMO is currently working on a new charging standard of up to 900 kW. Several stations have been opened around the world, but they are consistently for medium-sized trucks. Such as in California, where the American transport firm Penske has an HPCS with 14 charging points for Daimler Freightliner eM2 [1].

2.1.4 HDEV models

Today, most of the electric truck models are part of the light to medium segments, such as the Volvo FL Electric and the Freightliner eM2 [6], [7]. Several companies are planning to start mass-production of HDEVs in the upcoming years. It is different how many details are known about each model. The most prominent models are Tesla Semi and Freightliner eCascadia. The Freightliner eCascadia will have a battery with a usable size of 475 kWh and can charge up to 80% during 90 minutes, [3]. The given specifications imply a charging power of approximately 350 kW, which is already used for some EVs. Tesla Semi has a tremendous increase in battery size and charging power compared to today's norm. Based on the given driving range of 800 km, driving efficiency of 1.15 kWh/km, and some assumptions in charge and discharge efficiency of the battery, it is calculated that the battery size of the Tesla Semi should be approximately 1 MWh [8]. In order to be able to charge the battery equivalently to the stated 640 km in 30 minutes, the charging power is potentially 1.6 MW.

2.1.5 Status of HDEVs in Norway

The number of HDEVs in Norway today is low. According to SSB, 21 electric trucks were registered in 2019 [9]. Twelve of these were medium-sized trucks from EMOSS and mainly used in urban freight [10]. These trucks have a battery size between 52 and 300 kWh, giving them a 100-350 km driving range. The charging power is either 22 or 44 kW which is compared with most EVs quite low, [11].

It is expected that the number of HDEVs will increase in the coming years. The Department of Transport Economics has predicted that the electric share of LDVs and HDVs is 94.9 and 3.8%, respectively, in 2050 [12]. The low share of HDEVs is predicted due to the Departments' more optimistic view of the hydrogen technology for long-haul vehicles. Both Volvo, Renault, Scania, and MAN are expected to start delivering electric trucks to Norway in 2020-2022 [13]. However, the expected driving range is only up to 300 km, which is not that suitable for long-haul freight. Asko, a leading freight company of foods, has ordered 10 Tesla Semis and will be the opening shot for long-haul electric trucks in Norway. In addition, the Norwegian post service and Travel Retail Norway have ordered respectively 1 and 2 trucks, bringing the total up to 13 trucks, [14].

2.2 Impact on the power grid

A higher share of electric penetration in the transport sector will add greater challenges to the power grid. IRENA, [15] presents main findings from different studies done in European countries regarding an increased share of electric mobility. It states three main findings. Firstly, the increase in electricity demand due to EV charging is limited. In a scenario where 100 % of the road vehicle mobility is electric in Europe, the energy demand will only represent 10 % to 15 % of the total electricity production. Secondly, the peak demand will increase significantly, especially in the evening, if it is not distributed reasonably. Thirdly, the impact on distribution grids is significant. Studies in different European countries,, conclude that problems related to transformer loading, line congestion, and voltage quality will demand significant investments in the distribution grid.

2.2.1 Impact of electric transport in the Norwegian power grid

The findings presented in [15] corresponds with studies The Norwegian Water Resources and Energy Directorate (NVE) have performed. They have written two reports that investigate the effect of the increased share of EVs, buses, and ferries in the Norwegian grid, [16], [17]. The investigated scenario assumes that 50 % of the cars, two-thirds of the ferries, and all the buses operating in urban areas are electric. One of the main findings is that there will not be an energy demand problem but a power demand problem.

Cables and transformers were investigated to get an overview of the grid impacts. A cable using over 90 % and a transformer using over 120% of its rated capacity is considered congested. The scenario resulted in 115 congested components. 90 % of the congested components are transformers, which makes up 10 % of all transformers in the investigated areas. Loads associated with EVs congest most components. However, the congestion is relatively small. Overloads due to ferries exceed higher values and are thus a greater challenge. The overload is less than 5 MW in 55 % of the cases, while 10 % experience an overload of more than 20 MW. In 2030, 48 of the components will be congested independently of the introduction of more electric transport. The replacement of 28 of these components is already planned.

The reports conclude that the electrification of the transport sector will have a negligible impact on the transmission grid. Overall, peak loads will be slightly higher. Since the peak load from charging EVs rarely occurs at the same time as the peak load in the transmission grid, it will not be regarded as a problem. However, it will introduce challenges to the distribution grid in areas where the density of EV charging is high, and the capacity in the grid is limited. They suggest that smart charging and load shifting may reduce the potential challenges of EV charging.

2.3 Price structure of HPCS providers in Norway

In Norway, there is, as of July 2020, approximately 800 HPCS distributed among a various number of operators, such as Ionity, Fortum, Tesla, and MER, [18]. They provide charging powers in the range of 50 kW to 350 kW. In table 1, the corresponding charging prices are presented. The pricing schemes consider delivered energy, charging duration, or a combination of both. An essential similarity among the providers is that the pricing is fixed independent of the time of the day or geographical location. A benefit with fixed pricing rates is the predictable charging cost for the

customer. However, the benefit of predictable pricing compromises the ability to encourage the customer to deviate from its preferred behaviour.

Table 1: Charging prices at HPCS operators in Norway.

Operator	**Charging power $\geq$ 150 kW**	**Charging power $\geq$ 50 kW**
Fortum	5 kr per kWh	3,10 kr per min
Mer	1,25 kr per min. + 3,20 kr per kWh	1,25 kr per min. + 3,20 kr per kWh
BKK	1,25 kr per min. + 3,20 kr per kWh	1,25 kr per min. + 3,20 kr per kWh
Lyse	1,25 kr per min. + 3,20 kr per kWh	1,25 kr per min. + 3,20 kr per kWh
Tesla	2,57 kr per kWh	2,57 kr per kWh
Ionity	8,40 kr per kWh	
Circle K	4,99 kr per kWh	4,49 kr per kWh
Kople	1,25 kr per min. + 3,20 kr per kWh	1 kr per min. + 3,20 kr per kWh
Supercharge	1,25 kr per min. + 3,20 kr per kWh	1,25 kr per min. + 3,20 kr per kWh
E.ON	5 kr per kWh	4 kr per kWh

2.4 Demand response

As stated in section 2.2, the electrification of the transport sector is going to add challenges to the power system. The demand curve for the power system is becoming more volatile. Therefore, it is crucial to enhance energy and cost-effective methods to make the demand more stable and predictable. One of the methods that are considered the most cost-effective and reliable for smoothing the demand curve when the system is operating at its limit is demand response. This could be a tariff that encourages the customer to reduce its load when the market prices are high or when the grid reliability is threatened. Meaning that the demand response should benefit the customer and the power grid, resulting in an increase in social welfare. Reference [19] sums up the main objectives of demand response in four points. Firstly, to reduce the total electricity consumption. Reducing the customers' electricity usage also contributes to fewer losses in the transmission and distribution grids. Secondly, due to the reduced electricity consumption, less electricity is needed to be generated, causing lowered operational costs for the producer. Thirdly, changing the demand profile to follow the available power supply closer. Lastly, if the aforementioned is applied, the time with overloads will be reduced or removed, which is the primary motivation for applying demand response.

2.4.1 Demand response in terms of dynamic pricing

The demand response programs are divided into several groups. One such group is the price-based programs. As described in section 2.3, fixed electricity prices are the norm in the charging market today. Unlike the fixed pricing schemes, a price-based program will vary the prices throughout the day. Different price based programs are presented in [20]. They are presented in the context of household customers. However, the same principles can be applied to vehicle charging. *Real-time pricing* is a strategy that updates the price at different set time intervals, e.g. every 15 minutes or every hour. Often are the prices released to the customer an hour or a day ahead. In that way, the customer can plan its consumption. With the program *Time-of-Use Pricing* the price is also changing throughout the day. Unlike, real-time pricing the intervals are typically longer and fewer

during a day. The price in one time interval may be significantly higher than the others to shift the load to off-peak intervals. The pricing and defined time intervals are published well in advance and are kept unchanged for a long time, making it more predictable for the customers than real-time pricing. Another strategy is *Critical peak pricing*. This strategy follows the Time-of-use structure, except for times when the grid reliability is threatened. During those hours, the price is replaced with a predefined price that is much higher than the standard rates, which guarantees that the system will balance supply and demand.

2.4.2 Demand response requires flexibility

These price-based programs depend on usable flexibility in both the power grid and customer behaviour. In [21], several types of flexibility that can be utilised for demand response are addressed. One approach is to use the flexibility in the customers *schedule*. This method assumes that the customers' main requirement is to get the needed energy delivered. The time when this occurs is not that important. A customer may have some flexibility in *charging duration*. Using dynamic pricing schemes that favour longer charging duration makes it possible to reduce the charging power and thus reduce the peak load. If there is *spatial flexibility* present, it is possible to move the load from one location to another during times when a location suffers from, e.g. poor voltage quality or limited power supply. In this way, the system load do not necessarily reduce, but it can reduce the size of occurring voltage drops.

2.5 Load modelling

There have been conducted few studies on load modelling of high-power charging stations for HDEVs. However, the main principles are the same for load modelling of HPCS for EVs. Two different methods are mainly used in literature to build the load model. An agent-based approach is used in [22], [23], where each agent is operating autonomously according to one or several given objectives. Charging specifications, mobility pattern and vehicle type are defined for each agent. In [24], an agent-based model, which is initially developed for EVs in [25], is used to generate load profiles for HDEVs, by changing the input parameters. A second and more common method is to build the model on stochastic parameters without autonomous decision-making and interactions between the agents. References [26], and [27] are using Poisson processes with a predefined arrival rate or historical traffic flow data directly. The initial state of charge (SOC) is drawn from various probability distributions in [26]–[28]. In [29], SOC is not used as a parameter. Instead, data from HPCSs in Norway and Sweden containing charging duration is used. Monte Carlo simulations are often applied to evaluate the uncertainty of the stochastic parameters [24], [26], [27].

2.6 Grid impact

The authors in [24] have performed an analysis of the grid impact of HPCS for HDEVs. To look at vehicles with high enough charging power and battery capacity, HDEVs were defined as vehicles with a driving range of 400-800 km in a single charge. The investigated system had an HPCS with five charging points, à 1.2 MW, integrated. Time series analysis was used to investigate the grid impact. The analysis was conducted with the HPCS placed on different locations based on how suitable the connection point was. At the nodal location where there is sufficient capacity, the voltage never dropped below 0.95 p.u. At the nodal location where there is not sufficient capacity, the voltage dropped below 0.8 p.u.

Other literature focuses mainly on the impact of integrating charging of LDVs or HDEVs with shorter driving range, such as urban electric buses. In [30], the impact of electric buses has been analysed. The mobility model is based on a bus network in Vienna, Austria. During operational hours, buses are charged for a few seconds at every station or for several minutes at the end-stations of a bus line. The charging power is ranging between 300 and 600 kW. The results implied that most European cities should be capable of integrating lines with electrical buses.

In [31]–[33], the impact from charging EVs with a peak demand ranging from 0.7 to 2.5 MW is investigated. The main finding is that the voltages at times suffer from flickering. However, the voltage drop rarely causes any severe problem. In [32], a load profile with a peak demand of 2.2 MW is applied on a 34-node test feeder. The voltage deviation in the worst-case scenario is observed to be 6 %. The load profile implemented in [33] has a peak demand of 2.5 MW. Initially, the highest loading of the transformer is 80 %. After the addition of an HPCS for EVs, the maximum loading is raised to 90 %. The voltage at the weakest point in the power grid dropped from 0.95 to 0.93 p.u.

2.7 Dynamic pricing

The concept of dynamic pricing has been investigated in contexts regarding EV charging. However, it is conducted few studies that emphasise dynamic pricing in the context of high-power charging. A brief presentation of studies performed in the field is presented in the following paragraphs.

Several studies have investigated the concept of dynamic pricing regarding high power charging stations from the business owners perspective, [34], [35]. Thus, the charging station operator does not consider the optimal operation of the power grid but maximises its profit regarding the price scheme the utility provider has set. Typically a rate for the total energy demand and a rate for the peak load. The studies optimise regarding the long term revenue. The dynamic pricing is outperforming the fixed prices.

A dynamic pricing model to maximise the benefit for a microgrid is proposed by [36]. The optimisation problem considers the EV demand, charging and discharging time and source-load balance of the microgrid. The dynamic pricing strategy resulted in peak shaving and valley filling, causing more minor fluctuations in the load demand than the base scenario where fixed pricing was used.

References [23], [37]–[39] are all using dynamic pricing to shift the demand between the charging stations spatially. In [23] a rule-based dynamic pricing strategy is utilised. The charging price is updated according to the monitored voltage level at the connected bus. The price increases with decreasing voltage level to incentivise the customers to choose a different charging station. A dynamic pricing model that tries to uniformly distribute the EVs among all the charging stations in the system is presented in [39]. The objective of the optimisation problem is to minimise the overlap between residential load and EV load. The proposed model showed promising results and mitigated grid congestion. In [37] and [38] it is assumed that the customers respond to the dynamic prices both spatially and in energy amount. The optimised price profiles are generated by solving a stochastic dynamic programming problem where the objective is to maximise the charging providers' profit and the users' profit and negate the fluctuations in electricity consumption from the power grid.

To the best of the author's knowledge, it is today no real-life projects where dynamic pricing is applied to high-power charging stations. However, there are several projects that use dynamic price tariffs, at home chargers or other low power facilities to incentivise EV owners to charge their vehicles during off-peak hours, typically during nighttime. In the San Diego region, San Diego Gas and Electric have utilised a time-varying pricing scheme since 2016 to incentivise the customers charging activities during moments of high renewable energy injection to the power system [40]. Additionally, some projects have been launched in Spain, UK and Denmark [41].

3 Theory

This section gives an introduction to power flow analysis, optimal power flow calculations and agent-based modelling.

3.1 Power Flow

Power flow analysis comprises the steady-state analysis of an interconnected power system during balanced operating conditions. The following equations are obtained from [42].

In a network, the current injection is calculated from equation 1. All impedance elements in the system are gathered in the complex bus admittance matrix Y_{bus}. This matrix describes the relation between the current injection matrix I_{bus} and the bus voltage matrix V_bus.

$$I_{bus} = Y_{bus} V_{bus} \tag{1}$$

Equation 1 can be rewritten as equation 2. I_i is the current injection at bus i, and N is the number of buses in the system.

$$I_i = \sum_{k=1}^{N} Y_{ik} V_k \tag{2}$$

In a power system, the quantities of power are rather known than the quantities of currents. Thus, the current injection equation 2 is used to create corresponding complex power injections, equation 3 at each bus as a function of the bus voltage.

$$S_i = P_i + jQ_i = V_i I_i^* \tag{3}$$

These power injections are further balanced with the injections from the connected loads, S_i^L, and generators, S_i^G, at the bus i. Resulting in equation 4.

$$S_i + S_i^L - S_i^G = 0 \tag{4}$$

This complex power balance equation can be decomposed to the active and reactive power balance equations 5a and 5b by using the decomposed bus admittance parameters G_{ik} and B_{ik} and decomposing the voltage to the magnitude V and angle δ.

$$P_i(V, \delta) = V_i \sum_{k=1}^{N} V_k \left((G_{ik} \cos(\delta_i - \delta_k) + B_{ik} \sin(\delta_i - \delta_k) \right) \tag{5a}$$

$$Q_i(V, \delta) = V_i \sum_{k=1}^{N} V_k \left((G_{ik} \sin(\delta_i - \delta_k) - B_{ik} \cos(\delta_i - \delta_k) \right) \tag{5b}$$

In order to solve the set of power flow equations, some quantities at each bus must be known. In the power system, only two out of four quantities are known for every bus. Thus, each bus can

Table 2: Classification of buses

Type of bus	**Known**	**Unknown**
Slack bus	V, δ	P, Q
Load bus	P, Q	V, δ
Generator bus	P, V	Q, δ

be classified based on the known and unknown quantities, as presented in table 2. The unknown quantities are then found by solving the power flow equations 5. There are multiple ways of solving these equations. In this thesis, the equations will be solved by using the python package 'pandapower' that utilises the widely used Newton-Raphson method [43].

3.2 Optimal Power Flow

Optimal power flow (OPF) is a mathematical tool to find the optimal operation point of a power system at a given time step given constraints that maintain a feasible operation area and security, [44]. A power system contains multiple nodes, transfer lines, generators and loads, among other components. Each of these components has restrictions that must be met to operate the power system efficiently and safely. The power injection must be of equal size to the load demand and losses in the system. The general OPF formulation in its standard form is given in equation 6.

$$\begin{aligned}
&\min && f(x) && \text{(6a)}\\
&\text{subject to} &&&&\\
& && g(x) = 0 && \text{(6b)}\\
& && h(x) \leq 0 && \text{(6c)}\\
& && x_{min} \leq x \leq x_{max} && \text{(6d)}
\end{aligned}$$

In this problem formulation $f(x)$ is the the generation costs, $g(x)$ are the power balance equations in each node, while $h(x)$ are the inequality constraints regarding the transfer capacity of each line. Equation 6d are the upper and lower bounds for the control variables x.

The general OPF problem is usually solved by using one of two models. One approach is to use the nonlinear AC optimal power flow (ACOPF) model that uses the full AC power flow equations shown in equation 5. Due to the non-linearity present in the ACOPF method, it is commonly approximated by the linearised DC optimal power flow (DCOPF) . This approximation neglects the line losses and is not included in the nodal prices. In this thesis, a radial network with one power source will be investigated. Thus the inclusion of the line losses is desirable. Therefore, the ACOPF method is chosen for calculating the nodal prices.

The ACOPF problem will be formulated and solved using the same python package, 'pandapower'. The problem formulation and solver is the same as the one used in the open-source package MATPOWER in MATLAB [45]. In this ACOPF model, the control variable x consists of four variables stated in equation 7. δ_i and V_i is the voltage angle and voltage magnitude respectively

at node i, while P_i and Q_i is the active and reactive power at the same bus i.

$$x = \begin{bmatrix} \delta_i \\ V_i \\ P_i \\ Q_i \end{bmatrix} \tag{7}$$

The full optimisation problem formulation is presented in 8. The objective function, equation 8, is the sum of the polynomial costs functions, f_i^P and f_i^P, for active and reactive power injection from each generator. Equations 8b and 8c are the power balance equations, where which maintain the power injection at node i equals the sum of load demand and power flow to and from the node. The line flow S_l in line l is maintained within its boundary S_l^{max} by following the equation 8d. In the following equations, 8e - 8h the upper and lower bounds for the control variables are given.

$$\min \quad \sum_{i \in N} f_i^P(P_i^G) + f_i^Q(Q_i^G) \tag{8a}$$

subject to

$$P_i(V, \delta) = P_i^G - P_i^L \qquad \forall\, i \in N \tag{8b}$$
$$Q_i(V, \delta) = Q_i^G - Q_i^L \qquad \forall\, i \in N \tag{8c}$$
$$-S_l^{max} \leq S_l \leq S_l^{max} \qquad \forall\, l \in L \tag{8d}$$
$$P_i^{G,min} \leq P_i^G \leq P_i^{G,max} \qquad \forall\, i \in N \tag{8e}$$
$$Q_i^{G,min} \leq Q_i^G \leq Q_i^{G,max} \qquad \forall\, i \in N \tag{8f}$$
$$V_i^{min} \leq V_i \leq V_i^{max} \qquad \forall\, i \in N \tag{8g}$$
$$\delta_i^{min} \leq \delta_i \leq \delta_i^{max} \qquad \forall\, i \in N \tag{8h}$$

Nodal prices

From solving the OPF problem, the optimal values for the control variables are found. In addition, other parameters related to sensitivity analysis are calculated. In this thesis, it is the nodal prices that are emphasised and used in the dynamic pricing scheme. The nodal price is essential as it describes the marginal cost of supplying an additional electricity unit at a bus. It takes into account the grid condition. Thus it includes costs regarding power injection, transmission losses, and line congestion [46]. A power system with one primary power source and a radial structure will be investigated in this thesis. Thus, the cost of generating power and the line losses are the main contributors to the nodal price. One essential attribute of radial networks is that the nodal prices will increase with the distance to the primary source due to the accumulated line losses present to deliver the electricity unit to the bus.

3.3 Agent-based modelling

An agent-based model is used to recreate or predict complex phenomena such as traffic and market behaviour. By [47], agent-based models describe systems where objects, called agents, interact within a defined environment. The agents individually consider what actions they will do based on a set of rules set for each agent. This set of rules is the basis for the agents' behaviour and may be deterministic or stochastic. Every interaction an agent takes is either with another agent or with the environment itself. Every agent can typically take one out of several states, and the transitioning between the different states are usually caused by the agent-to-agent or agent-to-environment interactions, [48].

Reference, [47] states several benefits from using an agent-based model. Firstly is the ability to capture emergent phenomena resulting from the interactions, which is beneficial when the results of the whole system are more than just the sum of the different parts of the system. This is typically when the system consists of agents with nonlinear behaviour, e.g. when specific characteristics are described as thresholds, if-then rules or nonlinear coupling. The interactions between agents are often heterogeneous that may deviate from the aggregated behaviour flow equations predicts due to most equations assumes a homogeneous mix of objects. Another benefit is that it introduces a more natural way of describing the system. Since individual behaviour may be complex, it is often easier to describe the behaviour with a set of rules rather than mathematical equations. The agent-based model is beneficial to simulate traffic flow as the position of each agent is not fixed. The agents' behaviour and the environment's condition will affect the movement, causing the agents to operate as a flow.

4 Methodology

This section will present the agent-based model that is used in the thesis. The proposed OPF based dynamin pricing method will be described. In addition, the extensions on the agent-based model needed to introduce HDEVs, the proposed pricing method and an additional method of evaluating which HPCS is the cheapest will be explained.

4.1 Motivation

It is necessary to use a model that will incorporate time-varying parameters in order to utilise dynamic pricing and allowing the creation of different behaviours based on the conditions in the system at a specific time. In this thesis, an agent-based approach is used to allow different agents in the system to interact based on the condition of the system and the other agents. It is beneficial to use an agent-based model because f the positioning of the agents is not fixed and that the population of agents is not homogeneous. In addition, it is useful to use an agent-based model as it is easy to vary the price in the system throughout the day.

In [23], an agent-based model for simulating traffic and the impact on the power grid is presented. This model will be the basis for the traffic environment in work conducted in the thesis. The author has added extensions and new functionality to incorporate OPF calculations, a new dynamic pricing scheme and HDEVs. The original model will be briefly explained in section 4.2 to ease the understanding for the reader. Additionally, the extensions and new functionality is described in section 4.3.

4.2 Simulation model

The environment in the agent-based model consists of two different layers. The first layer is a representative street map of the investigated area. In this layer, the HPCS are represented as *ChargingStation agents* and are placed at fixed locations and is the environment that allows the *Vehicle agents* to move around and interacting with the charging stations. The second layer is the associated power grid in the area. It contains the loads from e.g. households, schools, stores, in addition to the HPCS loads. The two layers are connected through the ChargingStation agents, with a spatial location at both the street map and the power grid. The environment manages all the events, such as vehicle movement and charging sessions. In addition, it contains different agents, the vehicle and ChargingStation agents, as mentioned. In addition, a *TrafficGenerator* and an agent that monitors the power grid and updates the charging prices at HPCSs are found in the environment. The following subsections will explain how each agent is defined and which properties they have. An overview of how the agents, the street map and the power grid are communicating with each other is presented in figure 2.

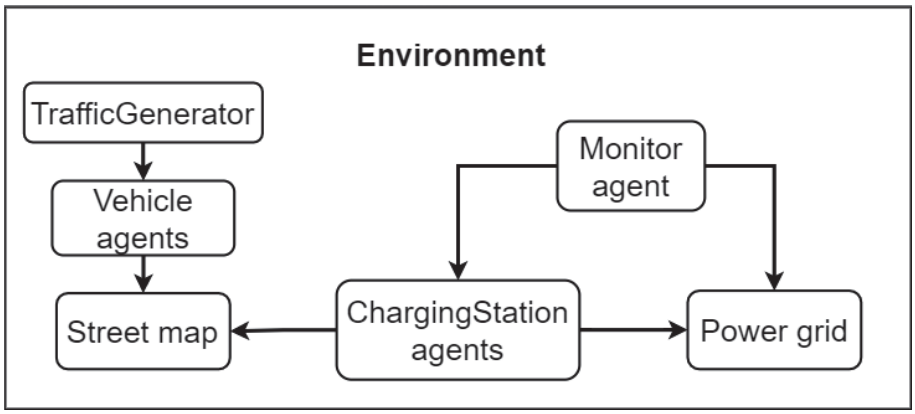

Figure 2: Overview of the relations between agents, street map and power grid.

4.2.1 Vehicle agents

The EVs are defined as agents that can move freely in the defined street area between their destinations in the model. Each vehicle is defined as either local or transient. The local vehicles belong to the area and have a defined home and workplace. The transient vehicles belong to areas outside of the investigated area and pass by along the highway. They are modelled to arrive at the system at specific entry points and leaving through defined exit points. Each transient vehicle may stop in the investigated area to charge if it is needed.

The vehicle agents are defined as Finite State Machines, meaning that an agent can only be in one out of a finite number of states. State transitions occur when the agent interacts with other agents or the environment itself. The different states for the vehicle agents are presented in table 3.

Table 3: Overview of the different states for the vehicle agents

States	**Local vehicles**	States	**Transient vehicles**
Home	The default location for the vehicle.	Entry	The location where the vehicle will enter the system area.
Work	Location for the destination the vehicle heads to every morning and return from after a working day.	Exit	The location of the vehicle's destination and where it will leave the system area.
Charging	The vehicle will search and drive to a HPCS if the SOC drops below the minimum level to reach its destination.	Charging	The vehicle will search and drive to a HPCS if the SOC drops below the minimum level to reach its destination.
Extra-trip	There is a probability that the vehicle will do an extra-trip on the way home from work. The probability is defined based on the vehicle type.		

In addition to the states, each vehicle agent has different parameters that define its attributes. These are the battery size, charging power, driving efficiency and a price preference parameter. The sizing of each parameter depends on the vehicle model it is assigned. Every time a vehicle need to charge, it will move to one of the available HPCSs. The selection will be made based on either price or distance. The price preference parameter, $price\_pref$, is a number between 0 and 1, depicting the vehicle's likelihood to select the cheapest HPCS. The greater the number, the greater

the chance the vehicle agent decides to go to the cheapest HPCS. This decision-making is done by drawing a uniformly distributed value u between 0 and 1. If equation 9a is fulfilled, the vehicle agent will choose the cheapest HPCS, while if equation 9b is fulfilled, the vehicle agent chooses the nearest HPCS.

$$u \leq price\_pref \tag{9a}$$

$$u > price\_pref \tag{9b}$$

4.2.2 ChargingStation agent

To represent HPCSs, ChargingStation agents are created. Each agent is defined by the number of charging points, maximum charging power and the charging price. The charging price can be updated dynamically based on the properties of the power grid. Each agent is assigned to a node in the street map and added as a load at a bus in the power grid. Thus, the ChargingStation agent is the connector between the two layers in the simulation environment.

4.2.3 TrafficGenerator

The TrafficGenerator agent generates the traffic in the system as given by its name. Before running the simulation, the number of local and transient vehicles must be defined. The population of the local agents are a fixed number set in advance and are created at the beginning of the first time step in the simulation. The transient agents follow an hourly traffic flow pattern based on a data set. The transient vehicles are generated and distributed uniformly during the following hour.

4.2.4 Monitor agent

The last agent is the monitor agent which its purpose is to monitor and follow the power system. Every time step, the agent will update the HPCS loads in the power grid according to the occurring charging events. After the update of loads in the power grid, the monitor agent initiates the power flow calculations. Furthermore, the monitor agent will evaluate whether the charging prices should be updated based on the condition of the grid.

4.3 Extensions and new functionalities to the model

To be able to model the desired system, which is further described in section 5, modifications and extensions are needed to be conducted. There are, in particularity, two main properties that lead to the extensions of the original model, the introduction of HDEVs and the new dynamic pricing strategy based on OPF calculations. Thus, changes have been made to several of the system agents. These are described in the following subsection. The new module that is running the OPF is presented in section 4.3.3. Additionally, another method of evaluating which HPCS is cheapest is introduced in section 4.3.4

4.3.1 Modelling a system with both EVs and HDEVs

It is desirable to distinguish the vehicle agents from each other, based on if they are EVs or HDEVs. This distinction is needed as the behaviour of EVs, and HDEVs differs, in addition to the vehicles seeks out different HPCS.

The vehicle agents are updated to include a new parameter, *vehicle_type*, that states if the vehicle is an EV or an HDEV. Due to the HDEVs investigated in this thesis are long haul trucks, their behaviour corresponds best to the transient vehicles. Thus, it is only the transient vehicles that can be assigned as an HDEV.

As stated in section 2.1.3 the charging powers that an EV and an HDEV utilises differ significantly in magnitude, and combined with the inequality in the physical sizing of the vehicles, it is natural to assume separate HPCSs will be established to serve EVs and HDEVs. Thus, it is necessary to distinguish the ChargingStation agents from each other in the same way as the vehicle agents. Thus an additional parameter, *cs_type*, is assigned to the ChargingStation agents, depicting if EVs or HDEVs can utilise it.

The TrafficGenerator agent is updated to create various types of traffic flows at multiple entry points. The traffic flow pattern of EVs and HDEVs differs from each other, and thus, it is a required extension of the agent.

4.3.2 Creating the power grid

As mentioned earlier, the second layer in the environment is the power grid. It is created by using the open-source package 'pandapower' in Python to conduct power flow analysis [43]. The power system is created by assembling 'pandapower' objects to get a grid representation. Using the built-in Timeseries module in 'pandapower', it is possible to iterate through time steps using the Newton-Raphson method, which allows for continuous power flow calculations as the monitor agent updates the load at each HPCS each time step. In addition to the HPCS loads, there are several base loads connected to the different buses. These are made by dividing the investigated area into different zones and aggregating the load from existing customers within a zone into a zonal load. The aggregated load demands are made by combining different demand profiles from, e.g. households, farms and schools. These load profiles are created in research done by SINTEF Energy, [49].

4.3.3 Dynamic pricing and OPF module

The OPF formulation presented in section 3.2 is solved to produce the price signals the proposed dynamic pricing strategy utilises. The implementation of the OPF calculations is created in a separate module that the monitor agent calls for every hour. A twin of the power grid is created in the OPF module to keep the power flow calculations separate from the OPF calculations. The twin power grid is also created using the python package 'pandapower'. The OPF problem is solved by using the interior point solver in 'pandapower'.

The twin network is updated with an artificial generator at each bus where a base load is connected. The maximal power production of the generator is equal to the size of the corresponding load at each time step. The power generation cost is set equal to a high rationing price. This add-on is done to maintain the feasibility of the OPF if the transfer capacity of a line or substation is maximised. The artificial generators will then start to inject power and thus reduces the load demand at the corresponding bus. In those cases, the nodal price will rise drastically, and the price set at the nearby HPCS is unfavourable, causing a more significant share of the traffic to move to other HPCSs.

It is essential to add the artificial generator as a static generator object and not a regular generator object. In addition, to regulate the power injection, a regular generator also sets a reference voltage magnitude and voltage angle, unlike a static generator which only regulates the power injection. It is not desired to control the voltage properties as the introduction is of the artificial generator is only to be able to reduce the load demand and introduce a rationing price.

To calculate the nodal prices, the monitor agent calls for the OPF module every hour. The monitor agent will then update the load parameters in the OPF problem before the OPF calculations are performed, which includes the upper bounds of the artificial generators that are equal to load demand in that time step at its associated bus. The remaining OPF parameters must be defined in advance as these are kept fixed for the whole simulation period.

The calculated nodal prices are obtained from the result matrix for buses to the associated power grid. The electricity price at each HPCS is set by scaling the nodal prices at the associated bus i with equation 10 to get an actual charging price, $C_{HPCS,i}$. C_{ref} is the reference price for what the HPCS operator demands for charging and is scaled with the ratio between the nodal price, λ_i, and the market price, C_{ext}, of energy delivered from the external grid. In this thesis, a pricing scheme that only prices the delivered electricity is utilised. It does not take into account the charging duration, which most HPCS operators do today, as presented in table 1.

$$C_{HPCS,i} = C_{ref} \frac{\lambda_i}{C_{ext}} \tag{10}$$

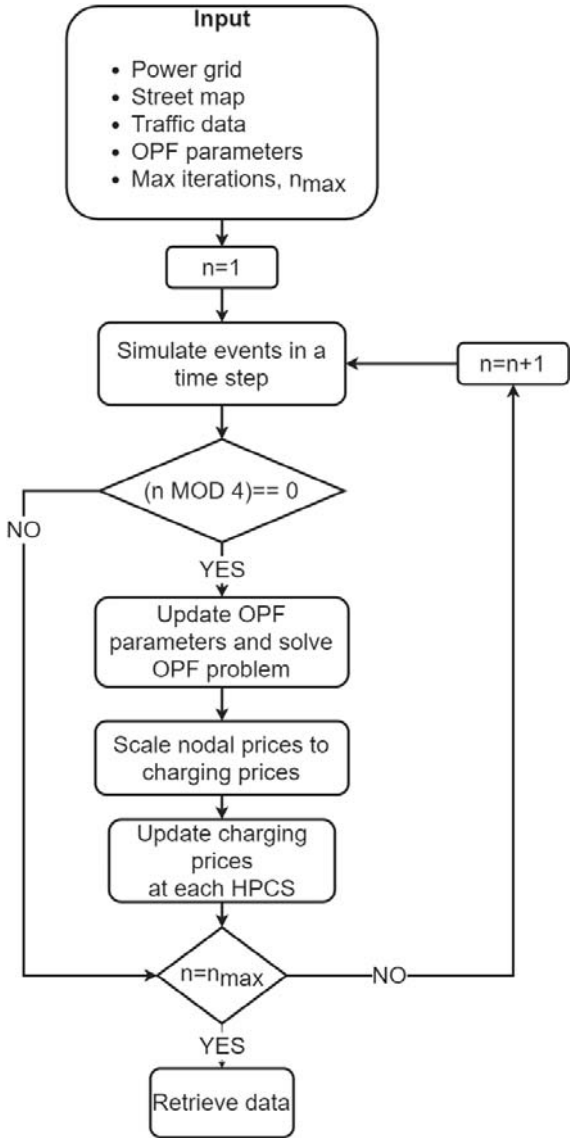

Figure 3: Flowchart of the model with OPF based dynamic pricing.

4.3.4 Introduction of a cost related to time of vehicle detour

In the original model, if the agent chooses the cheapest HPCS, it is only regarding the unit price for electricity. Since the distance to the different HPCS differs, the charging demand at an HPCS will differ due to the energy used to move from the agent's position when the decision was made. In addition to the extra electricity consumption, the time usage driving to the HPCSs will also differ due to the different distances. As for most people and companies, time is money. By adding a cost to the extra time spent driving to the HPCS, it is possible to prevent the agent to go to an unreasonable located HPCS. The benefit of choosing a cheap HPCS will vanish if it takes too much time and energy demand increases too much. Adding the cost of time and extra energy demand will recreate a more realistic driving behaviour. TØI is regularly doing calculations on how much a driver value the time spent driving an extra distance [50]. The following equations are added when evaluating which HPCS is the cheapest to include this behaviour to the vehicle agents.

To calculate both the extra energy and time spent driving to the HPCS, the length of the detour

must be calculated. The length of the detour via an HPCS, D, is calculated by using equation 11. Here $Dist$ is the distance from the current position to the destination, while $Dist_{HPCS}$ is the total distance to the destination via the location of the HPCS.

$$D = Dist_{HPCS} - Dist \tag{11}$$

The total cost C_{tot} by driving the detour is calculated by using equation 12. Here E is the initial energy demand for the vehicle at the current position, and η is the driving efficiency. C_{HPCS} is the electricity price at the HPCS, while v is the vehicle speed and C_{time} is the cost related to the extra time used.

$$C_{tot} = (E + D * \eta) * C_{HPCS} + \frac{D}{v} * C_{time} \tag{12}$$

5 System description and cases

In this section, a description of the investigated systems will be presented. First, the general characteristics of the system will be described. Then will each case with the corresponding adjustments be presented.

5.1 General system description

The area that is chosen to be the basis in the case study is Alvdal. Nearly 90 % of all the HDVs transporting goods between Oslo and Trondheim drives along the Norwegian National Road 3 through Østerdalen past Alvdal. In Alvdal, there is an established and designated lay-by area for HDVs and is, therefore, an interesting location to investigate grid impacts from HDEV charging. A day during the winter is used to create simulations that are challenging the power system the most. The current substation located in Alvdal has its highest loading during the winter.

5.1.1 Agent environment

The agent environment is created by using data from OpenStreetMap, with the coordinates of Alvdal and a radius of 6 km creates the area. In figure 4, an overview of Alvdal and its surroundings are presented. The green circles are marking the entry and exit points on the main road. In the cases presented in sections 5.2.1 - 5.2.3, the HPCSs for HDEVs are placed at location 1 and 2, blue circles. These HPCSs have a maximum operating capacity of 7 vehicles at the same time. In addition, an HPCS for EVs with a capacity of 20 vehicles is placed at location 1. This HPCS is an aggregation of the already existing HPCSs in Alvdal [51]. The red circle depicts the location of a remote location that is used to investigate the case presented in section 5.2.4.

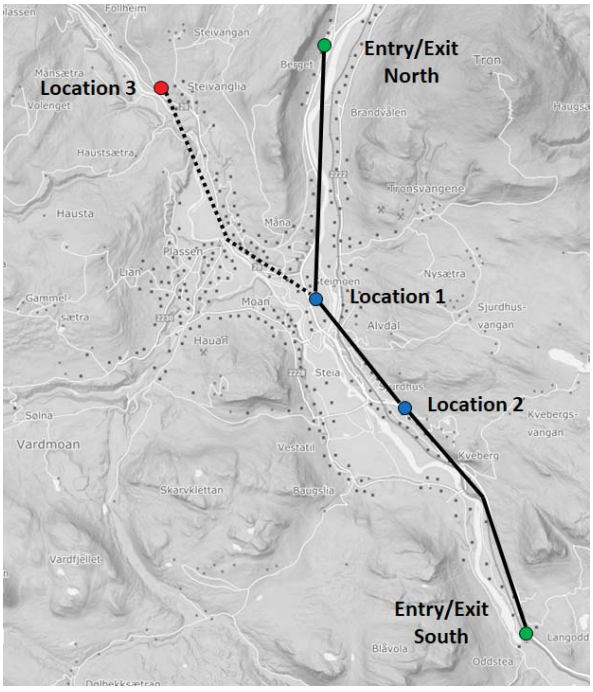

Figure 4: Overview of the HPCS locations and the entry and exit points at the main road.

The trafficGenerator's traffic flow input data is found from The Norwegian Public Roads Administration's traffic database, [52]. They have established measuring points in Alvdal that counts the vehicles passing by. The data set contains the hourly number of passing vehicles distinguished by the vehicle length. Personal cars are defined as vehicles shorter than 5.6 m and HDVs as longer than 16 m. The traffic flow from a sample day is shown in figure 5.

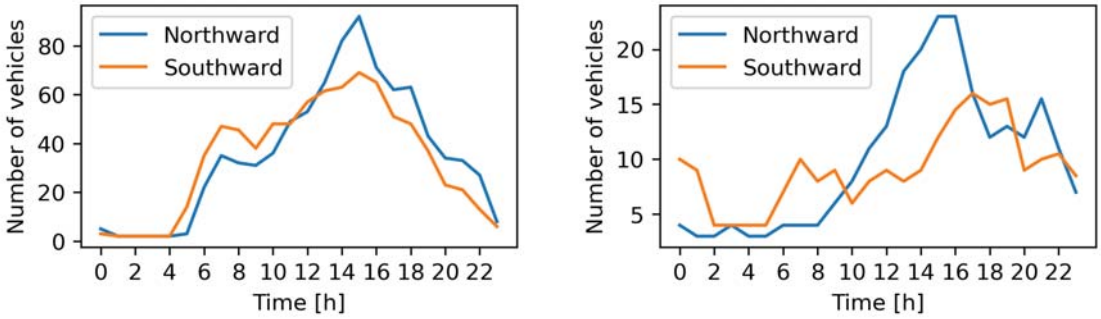

(a) EV

(b) HDEV

Figure 5: Traffic flow at day 25.

The specifications of each vehicle model are presented in table 4. It describes the battery size, charging power, driving efficiency and the share of the EV and HDEV population. The fleet of EVs is only represented with vehicles that charge with a minimum power of 110 kW to represent a future fleet of EVs. It is used, the six most sold EV models in between January and June 2021 in Norway, that satisfies that requirement. In this study, it is only used a generic HDEV model which has a charging power in between to upcoming HDEV models, Tesla Semi and Freigliner e-Cascadia, [2], [3]. The price preference parameter is set to 0.5 for the generic HDEV, while it is assumed to be of no interest for the EVs, as it is only be placed one HPCS that EVs can use in the investigated cases. The initial SOC level is set by assigning values from a uniform distribution between 20 % and 80 %. The vehicle agents will search for an HPCS if the SOC drops below 35%.

Table 4: EV and HDEV models

Vehicle model	**Battery size [kWh]**	**Charging power [kW]**	**Consumption [kWh/km]**	**Share [%]**
Audi E-tron	95	150	0,232	20
Volkswagen ID.4	82	125	0,188	20
Tesla Model 3	50	150	0,149	17
Volvo XC40	78	150	0,224	15
Mercedes-Benz EQC 400	85	112	0,216	13
Polestar 2	78	150	0,176	12
Generic HDEV	1000	1200	1,25	100

5.1.2 Power system topology

The exact power system topology is not fully known. However, a representative grid is made by using a map created by NVE, [53]. This map gives an overview of the power grid in Norway, except

for the lower voltage part of the distribution grid. The single line diagram of the power grid is presented in figure 6. The power grid contains 11 buses connected to the regional grid via a 66/22 kV substation transformer. The load customers in the area are divided into eight zones presented in figure 7. The aggregated loads are based on the number of units within each end-user group. A map made by Kartverket [54] has been used to distinguish the different buildings from each other. The resulting numbers for each end-user group are found in appendix A.

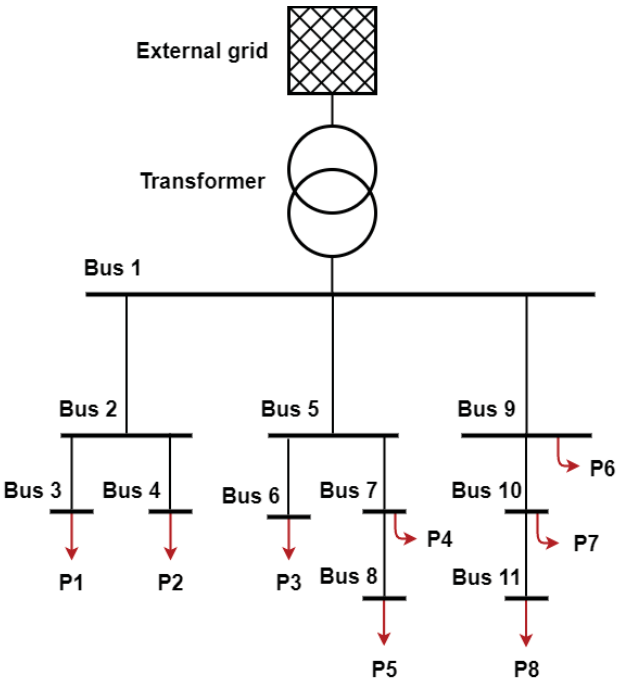

Figure 6: Single line diagram for the system topology without HPCSs.

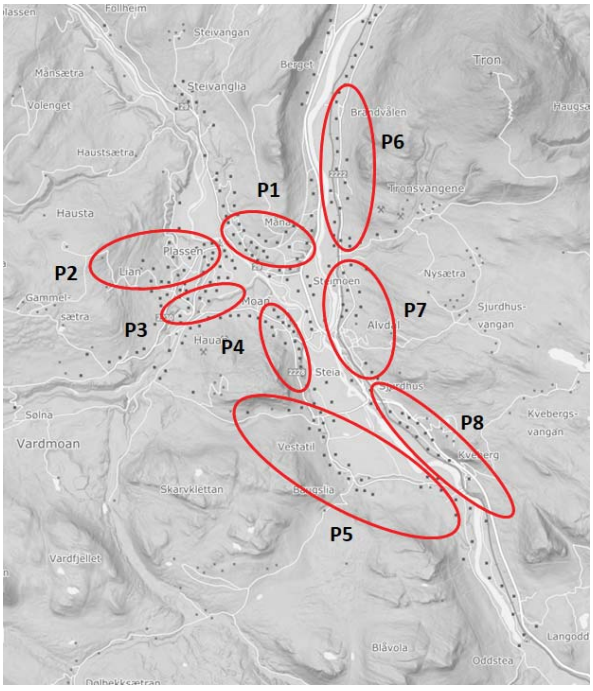

Figure 7: Location of the aggregated loads in the investigated area.

Topology 1

The first investigated topology is presented in figure 8. One HPCS for HDEVs is connected to bus 12, which is connected directly to the substation transformer. The other HDEV HPCS is connected to an extension of radial 5-7-8 at bus 13. Both HDEV HPCS loads are marked with blue. In addition, there is connected an EV HPCS to bus 12 as no other loads are located to this radial. The HPCSs for HDEVs will be referred to as HPCS 12 and HPCS 13 due to their connection to bus 12 and bus 13. The line parameters are presented in appendix A.

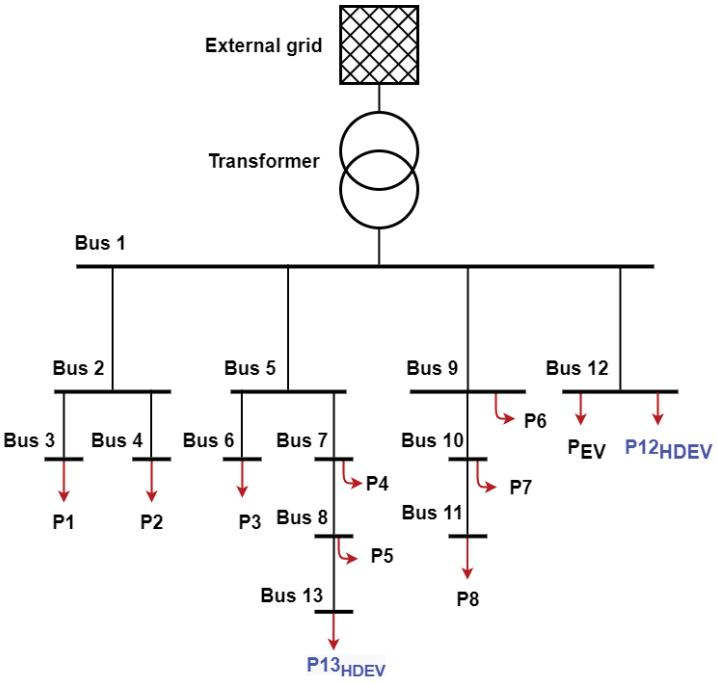

Figure 8: Single line diagram for power system topology 1.

Topology 2

The second investigated topology is presented in figure 9. Here the Bus 12, where the EV and HDEV HPCSs are connected, is in this topology no longer connected directly to the substation through its own radial. It is now connected with a line to bus 7, and thus the connection to the substation is weaker. Bus 13, containing the second HDEV HPCS, is moved from radial 5-7-8 and is now placed between bus 10 and 11, which is the radial having the highest load demand from the already existing loads in the system. The corresponding line parameters are found in appendix A.

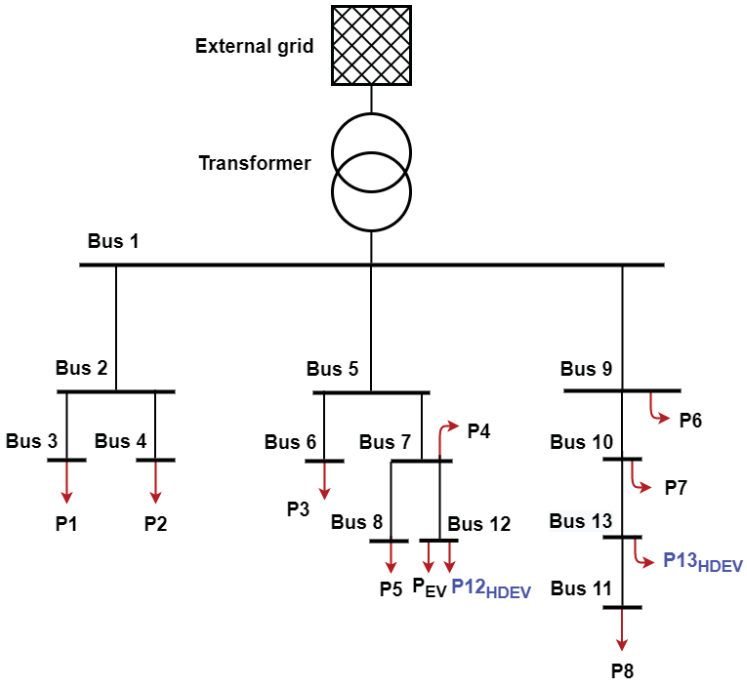

Figure 9: Single line diagram for power system topology 2.

5.1.3 OPF parameters

The OPF parameters are held the same for both power system topologies. An overview of the sizing of the OPF parameters that are needed to solve the OPF problem presented in section 3.2 is given in table 5. The price of an energy unit from the external grid, C_{ext} is set to be 50 kr/MWh. Each baseload has an associated generator as described in section 4.3.3. The rationing price, $C_{rationing}$, for each generator, is set to 1000 kr/MWh, while the maximum power injection is set equal to the baseload in each bus. The maximum transfer capacity to the substation and each line is set to 100 % of its rated capacity. The minimum and maximum voltage magnitude, V_i^{min} and V_i^{max} are set to 0.9 p.u. and 1.1 p.u. respectively. It is not set any boundaries on the voltage angles.

Table 5: Sizing of OPF parameters.

Parameter	Value	Unit
C_{ext}	50	kr/MWh
$C_{rationing}$	100	kr/MWh
S_l^{max}	100	%
$P_i^{G,min}$	0	MW
$Q_i^{G,min}$	0	MW
$P_i^{G,max}$	P_i^L	MW
$Q_i^{G,max}$	Q_i^L	MW
V_i^{min}	0.9	p.u.
V_i^{max}	1.1	p.u.

5.2 Price structure cases

Three different pricing structures will be investigated in the case study. Due to the price structures are dependent on the power system topology, they will be investigated for the two presented topologies. In addition, a case where the method to evaluate which HPCS is cheapest will be conducted.

5.2.1 Case 1: Fixed pricing

In the first case, a fixed pricing scheme is applied. The fixed pricing scheme is the same as some providers use today, only pricing the delivered electricity. The electricity price is set to 5 kr/kWh. Since there are no price deviations, the HDEVs are distributed evenly between the two HPCSs.

5.2.2 Case 2: Dynamic pricing - OPF

In the second case, the dynamic pricing strategy proposed in this thesis is applied. The electricity prices at the HPCSs is updated hourly regarding the nodal prices obtained from the OPF calculations. The vehicles that prefer price over distance will now choose the HPCS with the lowest electricity price. The reference price is set to 5 kr/kWh. In general, there is a threshold in price difference for when a customer wants to change a product. This threshold is not included in this model. The OPF can generate prices that have minor deviations from each other, which in reality might not be big enough for the customer to regard.

5.2.3 Case 3: Dynamic pricing - Voltage

In the third case, the dynamic pricing scheme proposed in [23] is applied instead of updating the prices regarding the nodal prices from the OPF calculations. The prices at the HPCSs is set after a pricing scheme based on the voltage magnitude at the connected bus. The different prices corresponding to each voltage magnitude interval is presented in table 6. When the price at each station is the same, the vehicle agent will go to the nearest HPCS.

Table 6: Charging prices corresponding to different voltage magnitudes.

Voltage magnitude [p.u.]	**Charging price [kr/kWh]**
0.96 <V	7
0.95 <V <0.96	11
0.93 <V <0.95	15
V <0.93	30

5.2.4 Case 4: Time is money

In the fourth case, a different method to evaluate which HPCS is the cheapest is applied. As described in section 4.3.4, a driver would not choose the cheapest HPCS without regarding the extra time that is spent. The extra time cost is set to be 560 kr per hour, which is according to

TØI, the valuation of extra time spent for good transport [50]. It is only the OPF based dynamic pricing scheme that will be investigated in this case.

The placement of the HPCSs is different from previous cases. In this case, the HPCS located with the strongest grid connection is placed further away from the main road, causing a detour to drive to the HPCS. Thus, the HPCS 12 is placed 6.35 km from the main road at location 3 in figure 4, which is resulting in a detour of 12.7 km in order to use the HPCS. It is assumed that the HDEVs will drive to the HPCS and then the same way back to the main road when the charging session is completed. The location of HPCS 13 is still at location 2. The new power system topology is equal to topology 2 presented in figure 8, except for the length of the line to bus 12 is increased to 5 km. The updated line parameters are found in appendix A.

6 Results

The system described in section 5 has been investigated using the model and pricing methods presented in section 4. Three different pricing schemes are investigated for two different power system topologies. For the first topology, the results from applying fixed pricing and OPF based dynamic pricing are presented and discussed in section 6.1.1 while the voltage based dynamic pricing results are presented in section 6.1.2. This is done to easier describe how the pricing schemes are impacting the system. The results from the second topology are presented in section 6.2. In this section, the results from all three pricing schemes are compared directly with each other as the main mechanics behind each method will be described in section 6.1. In section 6.3, the results from emphasising a cost related to taking a detour to get to the HPCSs is presented. In all sections, day 25 from the simulations is further investigated in addition to the simulations as a whole. This is done to highlight some of the phenomena that arise when applying dynamic pricing.

6.1 Topology 1

6.1.1 Comparing case 1 (Fixed) and case 2 (OPF)

The aggregated load profiles for the two HPCSs at day 25 with fixed and dynamic pricing are presented in figure 10. When fixed pricing is used, it is clear that the loading is evenly distributed between the two HPCSs. This result is as expected, as the vehicles are distributed evenly between the two HPCS in the fixed pricing case. The figure shows that HPCS 12 has the highest load peaks appearing between 17 and 20 when it reaches 4.8 MW. At HPCS 13, the load peak appears later at 22, with 3.6 MW. When the OPF based dynamic pricing strategy is applied, load shifting is present. The majority of the load shifting is from HPCS 13 to HPCS 12, which can be observed, e.g. during the morning hours 8 to 10 and between 17 and 19. Load shifting in the other direction is present between 19 and 21 when the load is moved from HCPS 13 to HPCS 12. This indicates the dynamic pricing impacts the load profiles.

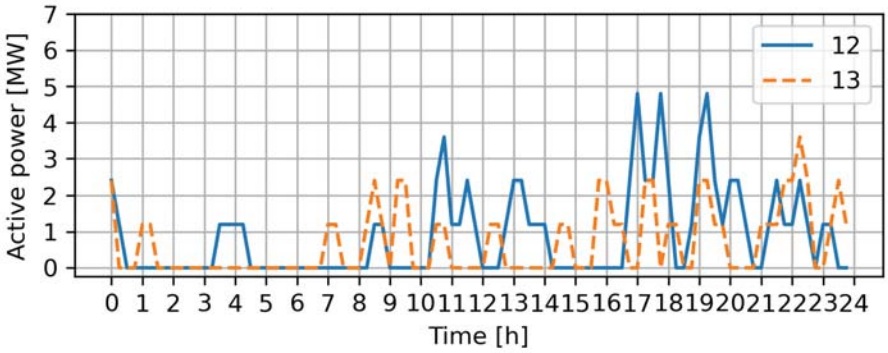

(a) Fixed pricing

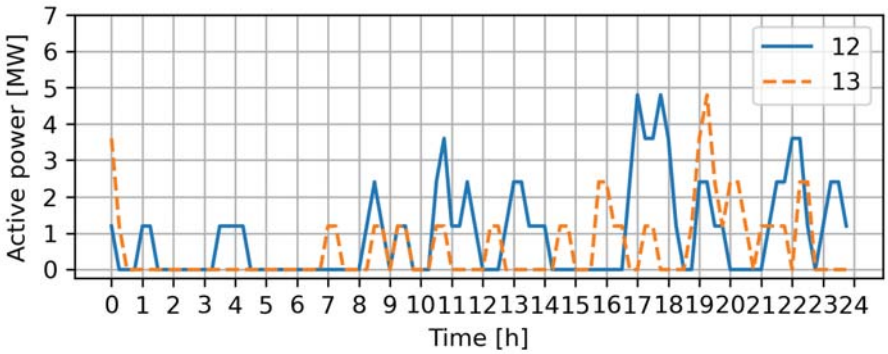

(b) OPF Dynamic pricing

Figure 10: Load profiles for day 25 at HPCS 12 and 13.

The price profiles for the two HPCS are shown in figure 11. The load shifting present in the load profiles is following the price profiles. During the hours between 8 and 10, the price at HPCS 13 is higher than the price at HPCS 12. This leads to a load shift between the two HPCS and causing the load at HPCS 12 to increase by 1.2 MW. Even though the price at HPCS 12 is higher than HPCS 13 between hours 17 and 18, the load increases at HPCS 12. This is due to how the monitor agent updates the prices at the HPCS. Every time the price in figure 11 steps at a whole hour, it is the value in the previous hour segment that will be observed price by the vehicles in that time step, and not the price in the following hour. Meaning the observed price at HPCS 13 at hour 17 by the vehicle is 5.06 kr/kWh and not 5.23 kr/kWh. This is due to the monitor agent updates the charging prices at the end of the time step each whole hour. Thus, the price at 17 is higher at HPCS 13 than HPCS 12, causing the vehicle agent to prefer HPCS 12. This is also the reason for the change in load at hour 19.

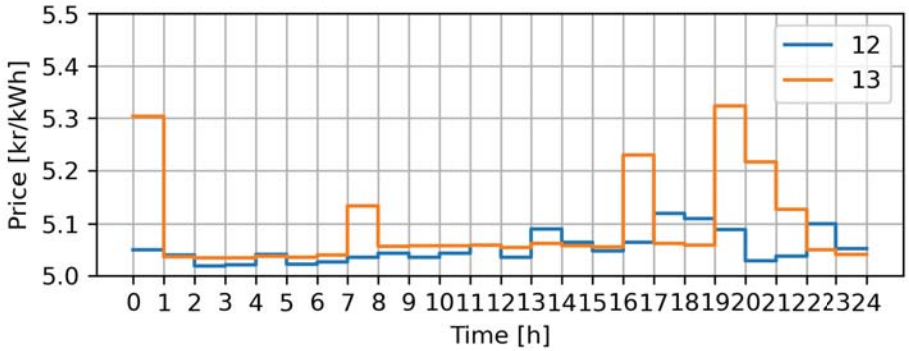

Figure 11: Price profiles at HPCS 12 and 13 at day 25 with OPF Dynamic pricing.

In figure 12, the average load profile from 100 simulated days are shown for both HPCSs and both pricing schemes. Since it is, in general, a small number of charging sessions during a day compared to the number of time steps (96), the average power demand at each time step is relatively low. However, the average profiles give an overview of how the load is distributed throughout the day. Similar to what is observed for day 25 in figure 10, it is clear that the load shifts from HPCS 13 to HPCS 12. During the hours between 01:00 and 08:00, HPCS 13 is barely used, and the load is shifted to HPCS 12. With the fixed pricing scheme, the peak hours at both HPCSs can be observed between 15:00 and 20:30. After applying the dynamic pricing strategy, the peak hours at HPCS are shortened by 2.5 hours and ends at 18:00. This results in the peak hours at HPCS 12 remain in time, but the power demand increases.

Table 7 shows the average number of charging events at each HPCS, and the average energy demand has moved between the two HPCSs. It supports the results from figure 12 that the load increases at HPCS 12, with an average of 3.3 MWh a day, while it is corresponding decreasing at HPCS 13.

Table 7: Daily number of charging events and energy demand.

HPCS	**Average number of daily charging events**		**Average daily energy demand [MWh]**	
	Fixed	OPF DP	Fixed	OPF DP
12	35	40	20.8	24.1
13	34	29	20.7	17.4

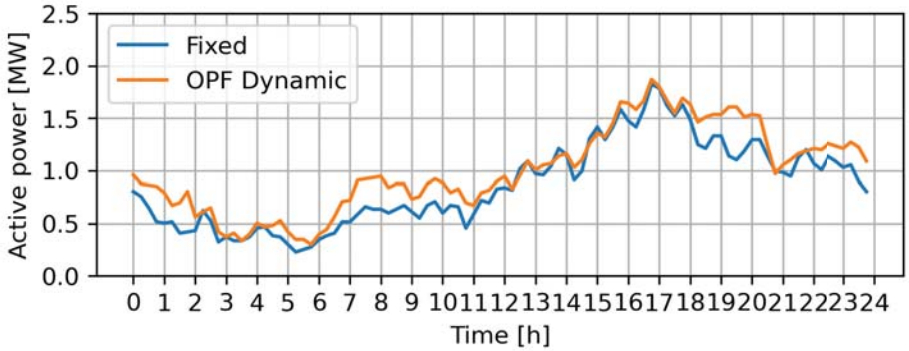

(a) HPCS 12

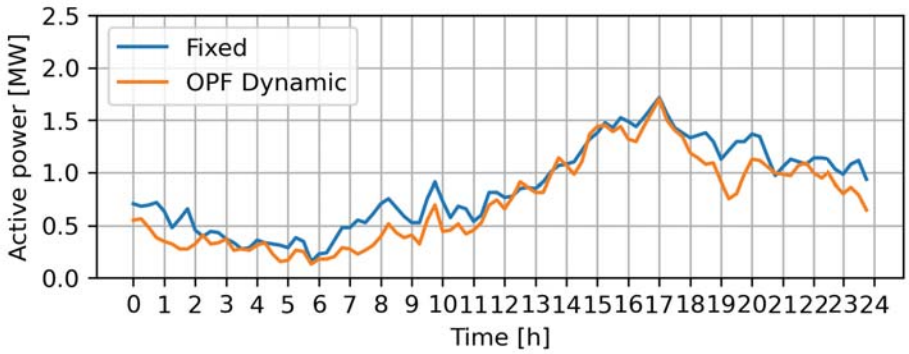

(b) HPCS 13

Figure 12: Average load profiles with fixed and OPF dynamic pricing.

One of the goals of using the dynamic pricing scheme is to utilise flexibility in the demand at one bus to reduce the voltage drop at another bus. As described earlier, bus 12 is connected to a radial with a strong connection to the transformer. There are no other loads than the HPCS for EVs that are connected to this radial. Thus, the voltage quality at bus 12 is good and can be regarded as a strong node. On the other hand, bus 13 is regarded as a weak node in this power system due to a more limited capacity in the radial connected to the transformer. It is desirable to increase the loading at bus 12, which withstands greater loads without causing the voltage drops to amplify to the same extent.

The introduction of HDEVs generates significant loads, as seen in figure 10. These new load demands cause voltage drops at various nodes in the power system. In figure 13, the voltage profiles for the two buses, 12 and 13, that are connected to the HPCSs are shown for day 25 with both pricing schemes applied. With the fixed pricing strategy applied, the voltage at bus 13 drops approximately 0.02 p.u. during most charging sessions, except at 22 when the drop is almost 0.03 p.u. Unlike bus 13, the voltage drops at bus 12 that are 0.01 p.u. or less.

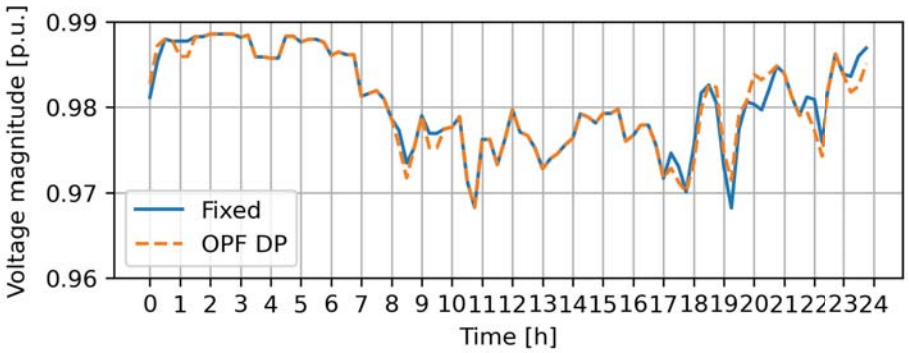

(a) Bus 12

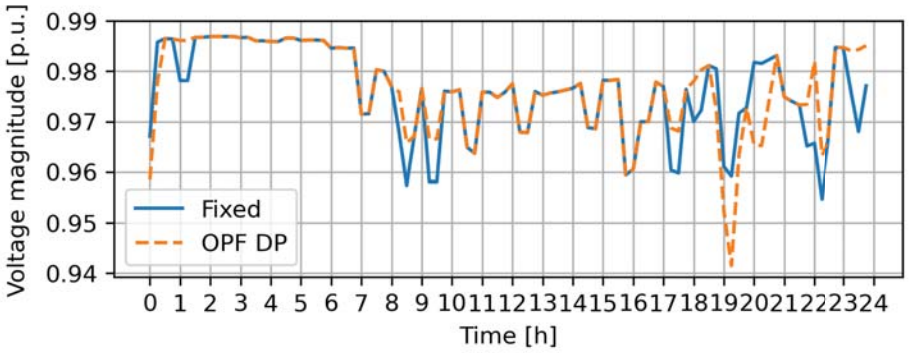

(b) Bus 13

Figure 13: Voltage profiles with fixed and OPF dynamic pricing at day 25.

The effect of applying the dynamic pricing scheme is quite clear. Due to the load shifting from HPCS 13 to HPCS 12, the voltage drops at node 13 have become smaller at several time steps. This is easily observed between 21 and 23, where the most significant voltage drop is observed with fixed pricing. The voltage is approximately 0.955 p.u. The voltage magnitude has with dynamic pricing increased with 0.01 p.u. and is now 0.965 p.u. In general, several of the voltage drops are removed or at least reduced at most time steps. These results are showing a good tendency with the dynamic pricing scheme. However, it can be observed an unfortunate event between 1830 and 1915 at HPCS 13. When the pricing is fixed, the voltage magnitude is 0.96 p.u. in comparison, it drops to nearly 0.94 p.u. when the dynamic pricing scheme is applied. The reason is that the price-setting is based on the grid condition in a previous time step and not how the load is expected to be in the next hour. Thus, the price set for each hour does not consider the load in the following hour when the price is applicable. This is the case at 1830. The observed price at HPCS 13 is based on the grid conditions at 18, which was more favourable to HPCS 13 as there were no charging events present, while three events were present at HPCS 12.

In figures 14 and 15, boxplots of the daily median and minimum voltage magnitudes are presented respectively for fixed and dynamic pricing at bus 12 and 13. The dynamic pricing, in general, has a positive impact on the voltage level at bus 13. The median voltage has increased at bus 13 and marginally decreased at bus 12, as seen in figure 14. However, the unwanted effect of amplifying certain voltage drops are present throughout all simulated days. This is resulting in the minimum voltage magnitude are equal to or worse at every simulated day as presented in figure 15. The main thing to take from these boxplots is that the dynamic pricing scheme is, in general, making

the voltage drops at bus 13 to be less, which is desired. However, the minimum voltage magnitudes have, in general, been decreased at bus 13. Thus the dynamic pricing amplifies undesired events.

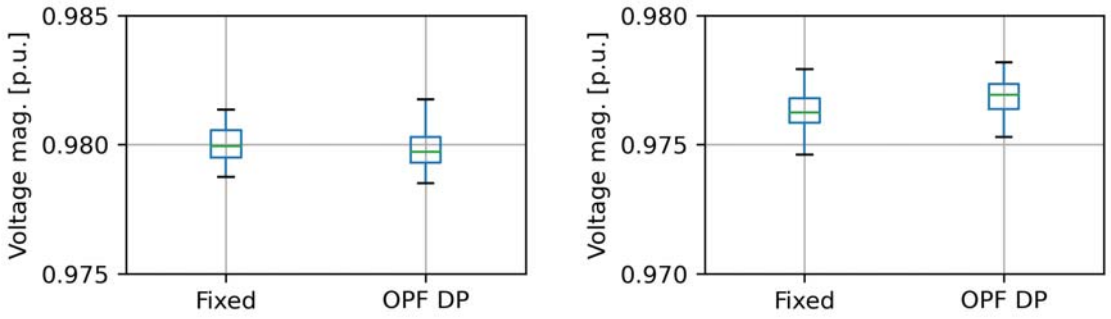

(a) Bus 12 (b) Bus 13

Figure 14: The daily median voltage magnitude for 100 simulated days with fixed and OPF dynamic pricing.

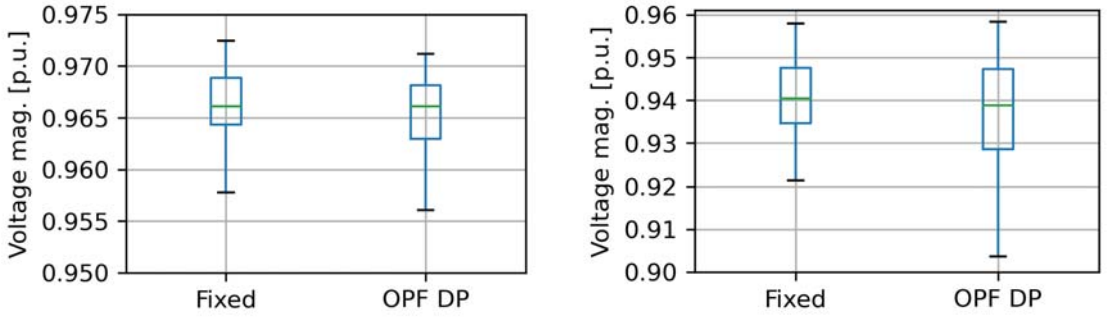

(a) Bus 12 (b) Bus 13

Figure 15: The daily minimum voltage magnitude for 100 days simulated with fixed and OPF dynamic pricing.

6.1.2 Comparing case 1 (Fixed) and case 3 (Voltage)

In this section, the voltage-based dynamic pricing scheme will be compared to the fixed pricing scheme. As with the OPF based dynamic pricing scheme, the voltage-based dynamic pricing strategy does also cause a load shifting between the two HPCS as seen in figure 16 for day 25. Throughout the day, most of the load shifting is from HPCS 12 to HPCS 13, except for the time around 19 when the charging demand at HPCS 12 increases by 2.4 MW. Interestingly, with this pricing scheme, most of the charging sessions move from HPCS 12 to HPCS 13. The average load profiles, shown in figure 17, substantiates this. Here it is clear that the average loading increases at HPCS 13 and decreases at HPCS 12. This is unlike the OPF based dynamic pricing scheme, which shifted the load from HPCS 13 to 12. It is necessary to investigate the voltage profiles and charging prices at each HPCS to understand why the load shifting has changed direction.

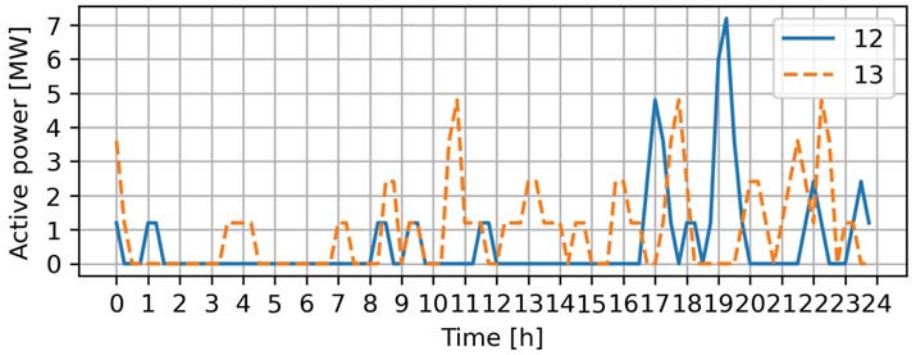

Figure 16: Load profiles for day 25 at HPCS 12 and 13 with voltage-based dynamic pricing.

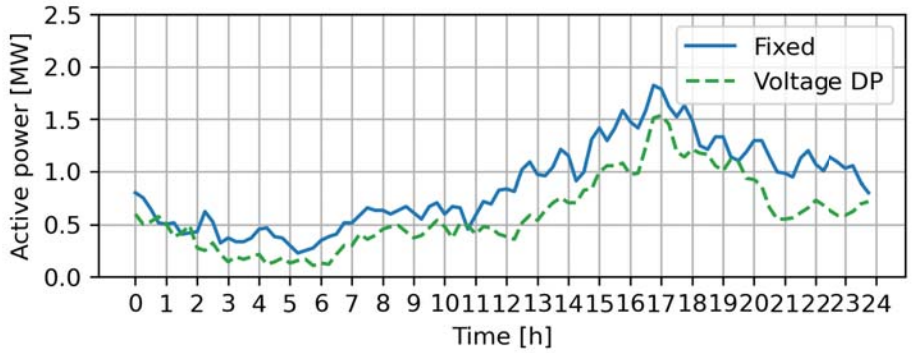

(a) HPCS 12

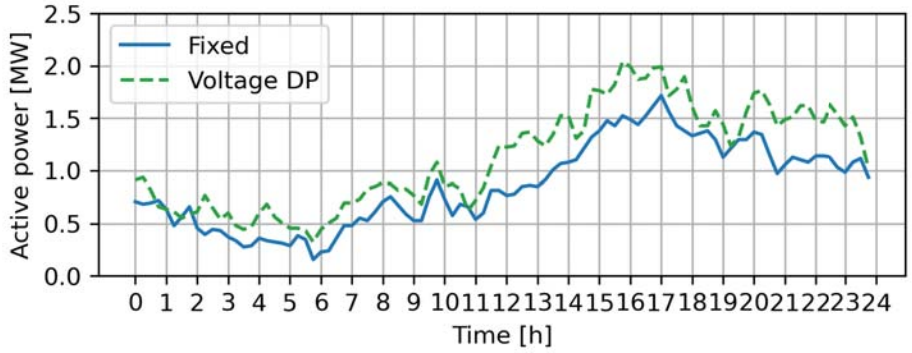

(b) HPCS 13

Figure 17: Average load profiles with fixed and OPF dynamic pricing.

Table 8 shows the average number of charging events at each HPCS, and the average energy demand has moved between the two HPCSs. It supports the results from figure 12 that the load increases at HPCS 13, with an average of 6.4 MWh a day, while it is corresponding decreasing at HPCS 12. Thus, it is moved almost twice as much energy demand between the two HPCS with voltage-based dynamic pricing compared to OPF based dynamic pricing. It is important to note that the load shift is in the other direction this time.

Table 8: Daily number of charging events and energy demand.

HPCS	Average number of daily charging events		Average daily energy demand [MWh]	
	Fixed	Voltage DP	Fixed	Voltage DP
12	35	24	20.8	14.4
13	34	45	20.7	27.1

From figure 18, it can be observed that the charging price at HPCS 12 is fixed for the whole day, at 7 kr/kWh. On the other hand, the price at HPCS 13 is varying throughout the day. The price at HPCS 12 is fixed because the voltage at bus 12 is never below 0.96 p.u. as seen in figure 19. The voltage at bus 13 has large voltage drops, causing the magnitude to be less than 0.95 p.u. and 0.96 p.u. at specific time steps, e.g. around 11 and around 18. This is causing the charging price to rise due to the pricing scheme defined in section 5.2.3. These voltage drops are due to how the vehicle agents respond to cases where the charging price is the same. In the occurrence of equal pricing, the agent chooses the nearest HPCS. From the traffic flow showed in figure 5 it is evident that the traffic flow from the south is greater than the traffic flow from the north in most hours between 9 and 22. This causes many vehicles to charge at HPCS 13 when the prices are equal since it is the southernmost located HPCS. With this system topology, the voltage-based dynamic pricing has resulted in an overall worse voltage profile than with the fixed pricing scheme.

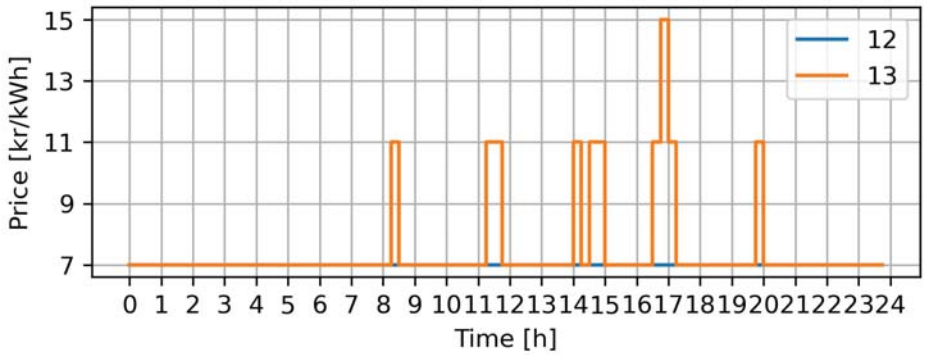

Figure 18: Price profiles at HPCS 12 and 13 with voltage dynamic pricing.

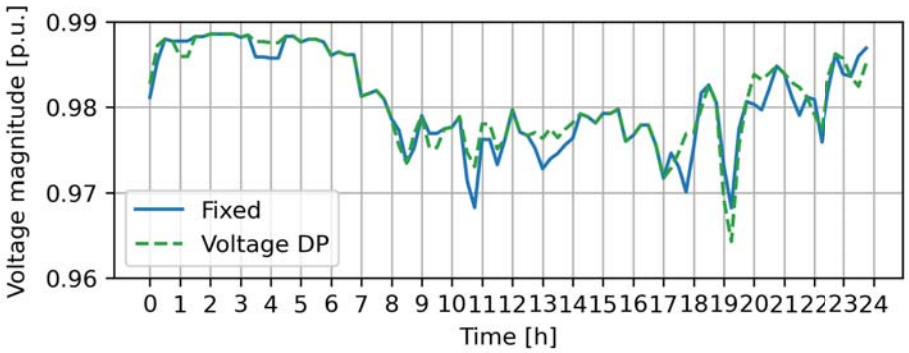

(a) Bus 12

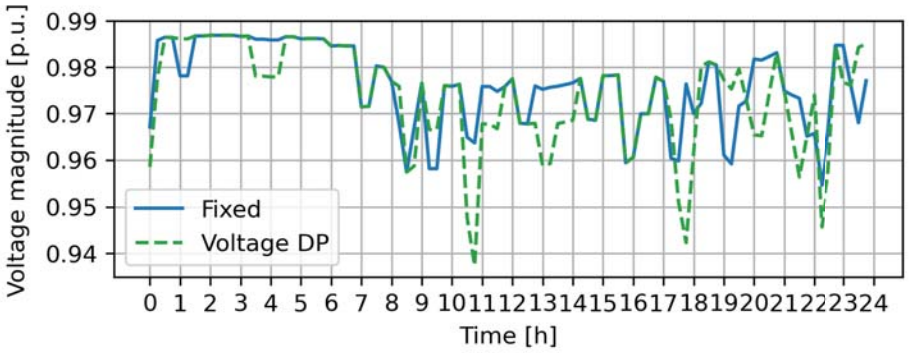

(b) Bus 13

Figure 19: Voltage profiles with fixed and voltage dynamic pricing at day 25.

The figures 20 and 21 are showing that both the median and minimum observed voltage levels at bus 12 have throughout the simulated days increased. The median voltage has been slightly reduced at bus 13, while the minimum magnitudes have been reduced significantly. This corresponds with the amount of load shifted from HPCS 12 to HPCS 13 with the voltage-based dynamic pricing. Increased load at bus 13, decreases the voltage magnitude.

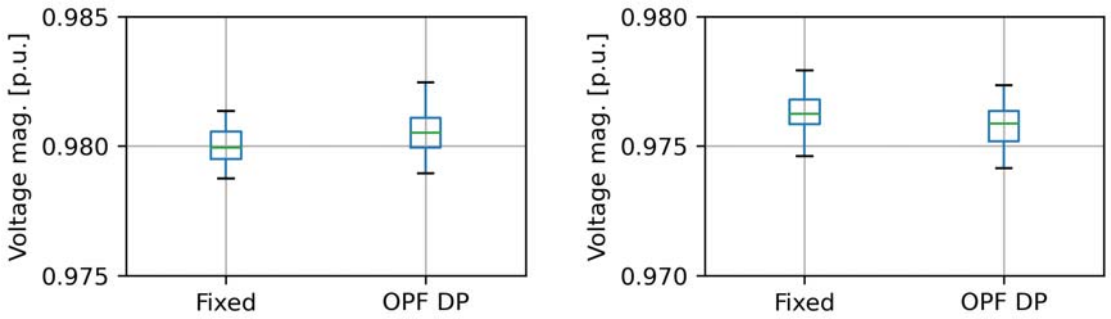

(a) Bus 12

(b) Bus 13

Figure 20: The daily median voltage magnitude from 100 days simulated with fixed and voltage dynamic pricing.

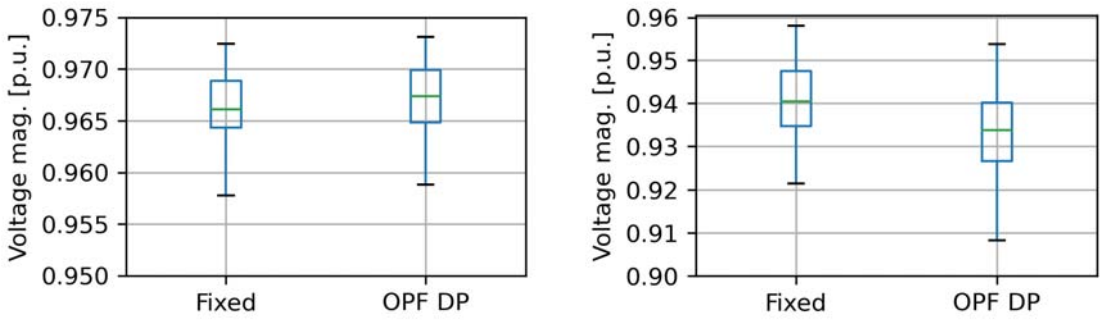

(a) Bus 12

(b) Bus 13

Figure 21: The daily minimum voltage magnitude from 100 days simulated with fixed and voltage dynamic pricing.

6.1.3 System losses in topology 1

The losses in the system are changed by moving the load between the two HPCSs. From figure 22 it is evident that applying the OPF dynamic pricing is having a negligible effect on the system losses. In the fixed pricing case, the average losses are 4.37 %, while with the OPF dynamic pricing, the losses have decreased to 4.36 %. However, the voltage based dynamic pricing has increased the losses slightly to 4.43 %.

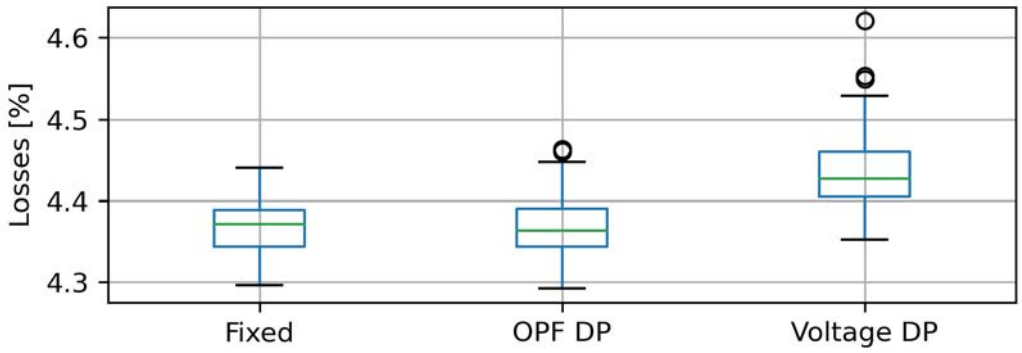

Figure 22: Average daily system losses for fixed pricing, OPF dynamic pricing and voltage dynamic pricing.

6.2 Topology 2

6.2.1 Comparing case 1 (Fixed), case 2 (OPF) and case 3 (Voltage)

Another topology has been investigated because both dynamic pricing schemes depend on the power system topology and loading condition. Since the spatial location of the HPCSs has not changed, the load profiles with fixed pricing are the same as the ones seen in the earlier presented figure 10. However, the loading profiles with the two dynamic pricing schemes applied are changed. In figure 23, it can be observed that the load profile with the OPF based dynamic pricing scheme is identical with the voltage based scheme, except for the period between 3 and 5, and the period between 21 and 23. In those periods, a greater amount has been moved to HPCS 13 with voltage-based pricing in comparison with the OPF dynamic pricing.

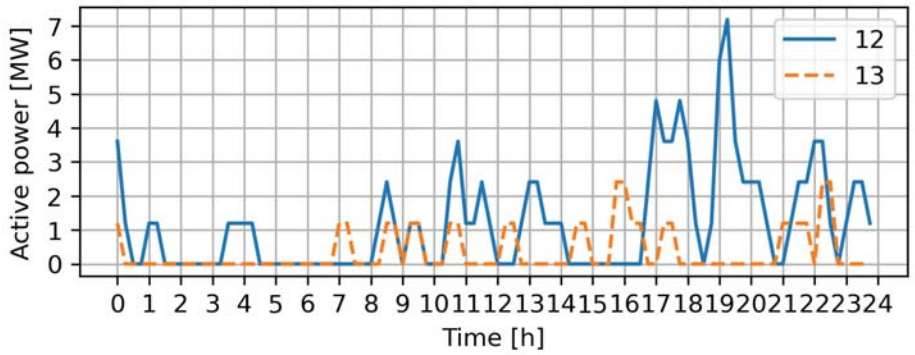

(a) OPF Dynamic pricing

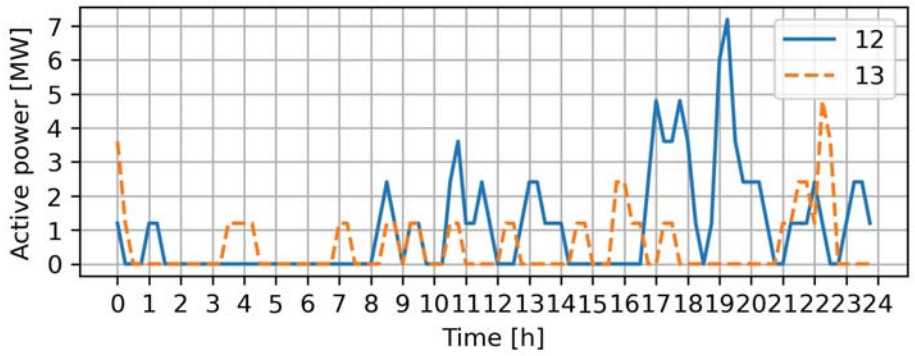

(b) Voltage Dynamic pricing

Figure 23: Load profiles for day 25 at HPCS 12 and 13.

The effect of changing the power system topology has a significant impact on how the voltage based dynamic pricing scheme affects the loading profiles, as seen in figure 24. The load shifting present is now majorly moved from HPCS 13 to HPCS 12. This shift causes the two dynamic pricing schemes to have a more similar impact on the load demand. Both load demands are now following the same profile between 5 and 21. This is because the charging price profiles follow a more similar pattern with this power system topology than the original power system topology. In the first topology, the price profiles for the two HPCSs were interchangeably the cheapest with OPF based dynamic pricing, figure 11. In the case of voltage based dynamic pricing, the prices are in most time steps equal, except for small time intervals, figure 18. The new power system

topology has made the prices profiles for the OPF dynamic pricing to always set HPCS 12 cheaper than HPCS 13, as seen in figure 25. This is resulting in a greater amount of the load is shifted to HPCS 12. The price profiles with the voltage based dynamic pricing are now getting closer to the OPF based dynamic pricing as the intervals with the lowest price at HPCS 12 are now lasting longer and causing the charging price at HPCS to be less than the charging price at HPCS 13 between 7 and 20 in both cases. This makes the demand profile between 8 and 21 identical for the two dynamic pricing schemes.

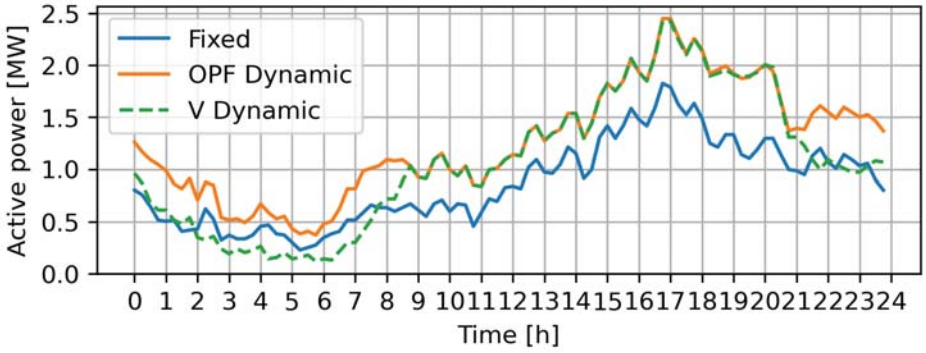

(a) HPCS 12

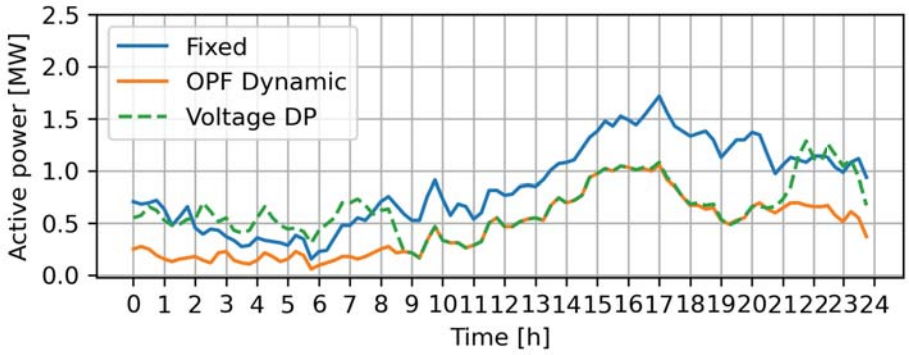

(b) HPCS 13

Figure 24: Average load profile with fixed pricing, OPF dynamic pricing and voltage dynamic pricing.

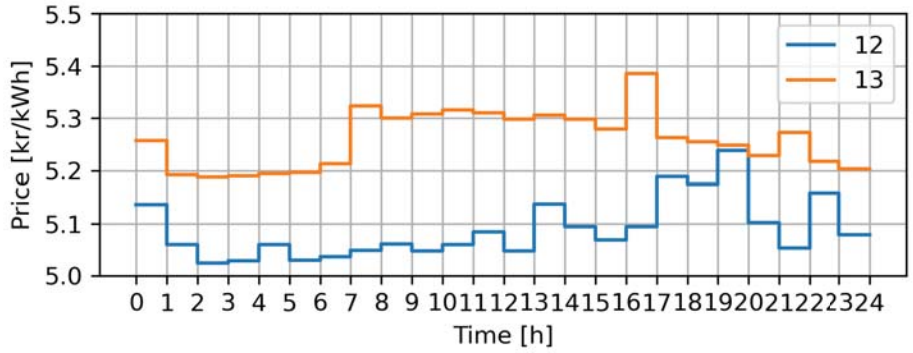

(a) OPF Dynamic pricing

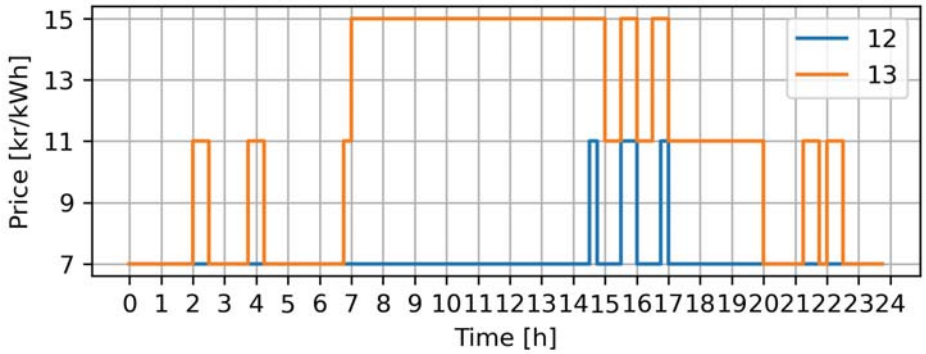

(b) Voltage Dynamic pricing

Figure 25: Price profiles for day 25 at HPCS 12 and 13.

In this power system topology, the voltage drops are either the same or less for the whole day with the OPF dynamic pricing scheme at bus 13, as seen in figure 26. Since HPCS 12 is always cheaper than the other one, the occurrence of amplifying the voltage drop at 19 is removed. The voltage profile for the voltage based dynamic pricing has had a better impact on the voltages than before. During the time between 7 and 21, the voltage drops are reduced or the same. However, some voltage drops outside of this time interval have amplified. This is due to the equal pricing of the HPCSs, 25, resulting in some vehicles choosing the nearest HPCS, which in this spatial configuration often occurs to be HPCS 13.

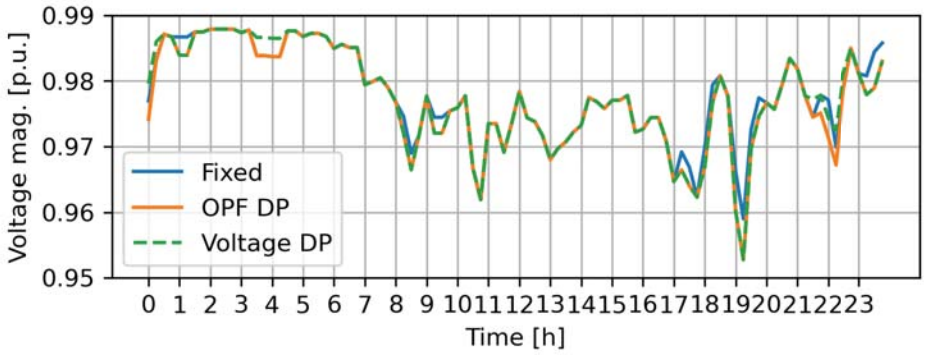

(a) Bus 12

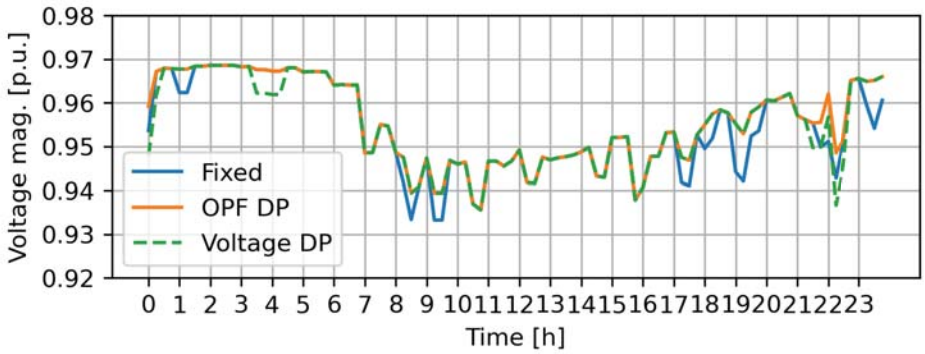

(b) Bus 13

Figure 26: Voltage profiles at day 25 with fixed pricing, OPF dynamic pricing and voltage dynamic pricing.

From figures 27 and 28, it is evident that the OPF based dynamic pricing scheme performs better in topology 2 compared to topology 1. The daily average voltage level has increased compared to fixed pricing as it did with topology 1. In addition, the occurrence of amplifying certain voltage drops and causing the daily minimum voltage levels to decrease have been removed. In topology 2, the minimum voltage is consistently higher at bus 13 compared to topology 1. The same observations can be done for the voltage based dynamic pricing. However, the positive impact on the average and minimum voltage magnitudes are slightly less. This is mainly due to the load shifting, appearing outside of the time interval 9-21, from HPCS 12 to HPCS 13.

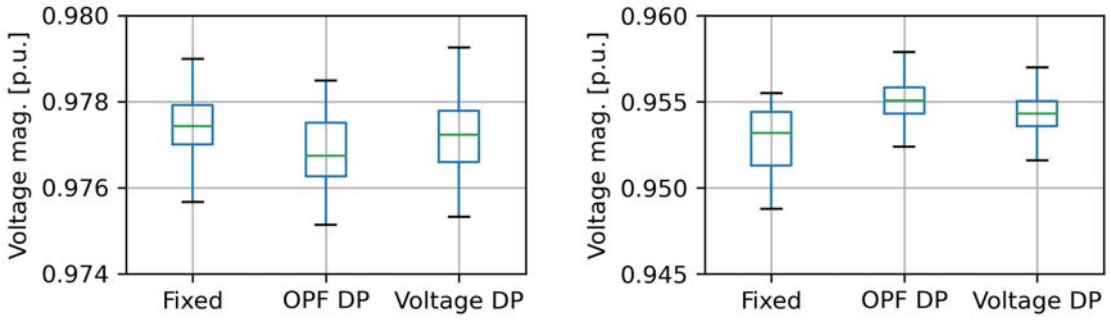

(a) Bus 12 (b) Bus 13

Figure 27: The daily median voltage magnitude from 100 days simulated with fixed pricing and OPF dynamic pricing and voltage dynamic pricing.

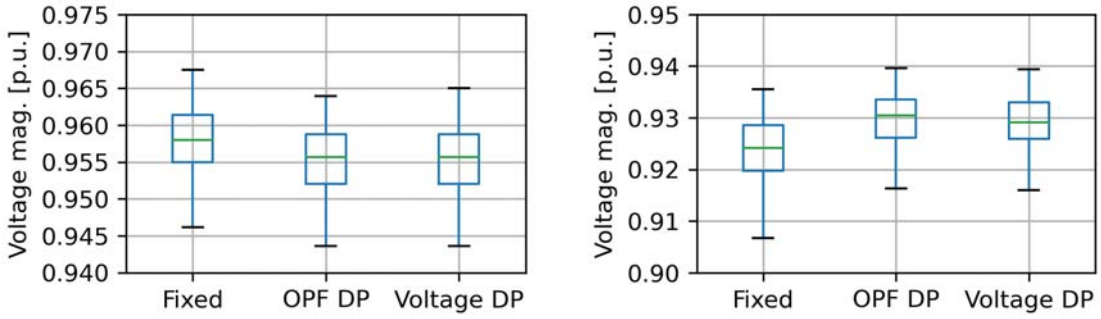

(a) Bus 12 (b) Bus 13

Figure 28: The daily minimum voltage magnitude from 100 days simulated with fixed pricing and OPF dynamic pricing and voltage dynamic pricing.

6.2.2 System losses in topology 2

The dynamic pricing schemes have had a positive impact on the system losses in topology 2, as seen in figure 29. The average system losses with fixed pricing are 4.74 %, while it is reduced to 4.57 % and 4.64 % respectively for the OPF and voltage-based dynamic pricing. This is a reasonable result as a greater share of the load is moved to a bus with a stronger grid connection, causing the transfer losses to reduce. The results are also reasonable in terms of more reduced losses with OPF dynamic pricing applied compared to applying voltage-based dynamic pricing. After all, the OPF price signals are generated from an OPF problem that its objective is to reduce the power injection to the system. Thus, indirectly reducing the system losses. The price signals from the voltage-based dynamic pricing do not reflect the system losses to the same extent.

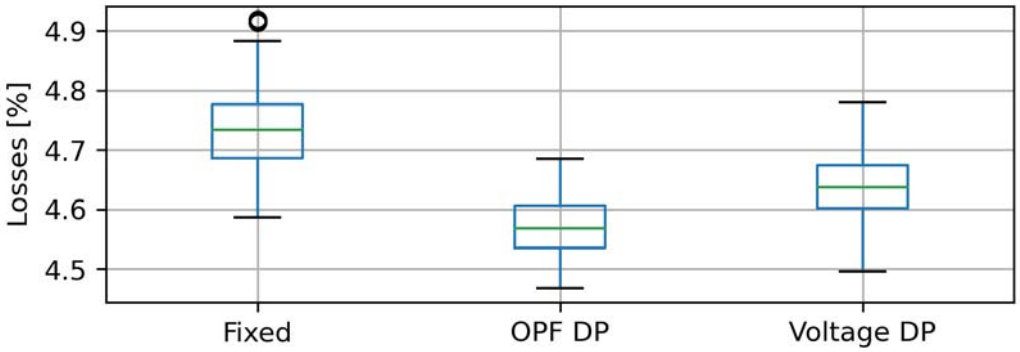

Figure 29: Average daily losses for fixed pricing, OPF dynamic pricing and voltage dynamic pricing.

6.3 Case 4: Time is money

The introduction of a cost related to time does not impact the load profiles in topology 1. This is due to none of the HPCSs are demanding a detour to get to them, since both HPCSs are located along the main road at location 1 and 2, seen in figure 4. This causes the variable, D, in equation 12 to be zero and resulting in equation 13. The remaining expression is then solely dependent on the charging price at the HPCS due to the initial energy demand E is fixed for each vehicle. This is causing the evaluation of which HPCS is cheapest to be equal with both decisions strategies.

$$C_{tot} = E * C_{HPCS} \tag{13}$$

To demonstrate the impact of considering the cost of time usage, HPCS 12 is placed at location 3 to introduce a detour of 12.7 km. Figure 30 are showing the load profiles for the two different methods of evaluating which HPCS is cheapest at day 25 from the simulations. It is evident that in this case, with the set locations and time cost, some charging events are moved from HPCS 12 to HPCS 13. This is easily seen in the interval 18 to 21. From these results, it is clear that the introduction of a cost for extra time and considering extra energy demand due to the detour impact the load profiles. It is causing the advantage of the low price at HPCS 12 to be not that dominant. From these results, it is, however, difficult to say which parameters in equation 12 is making the difference in total cost between the two HPCS to be in favour of HPCS 13 on the different occasions since the cost is depending on the initial energy demand for the specific vehicles at each occasion.

Further analysis is needed to be conducted on this method of evaluating which HPCS is the cheapest. The equation 12 is highly dependent on the extra distance to each HPCS and the price difference. Thus, a sensitivity analysis should be performed on the different parameters to understand better how the pricing scheme should be tuned.

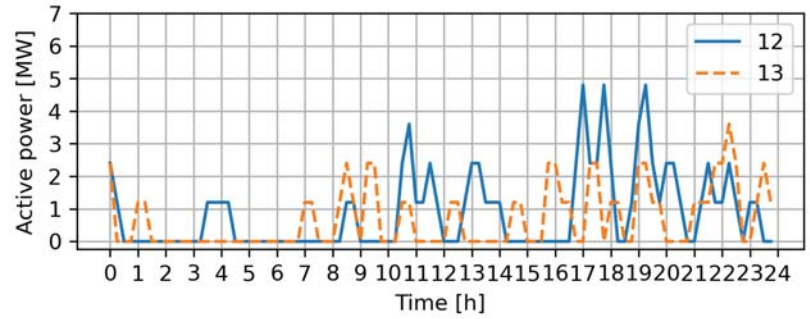

(a) HDEVs are only evaluating the charging price.

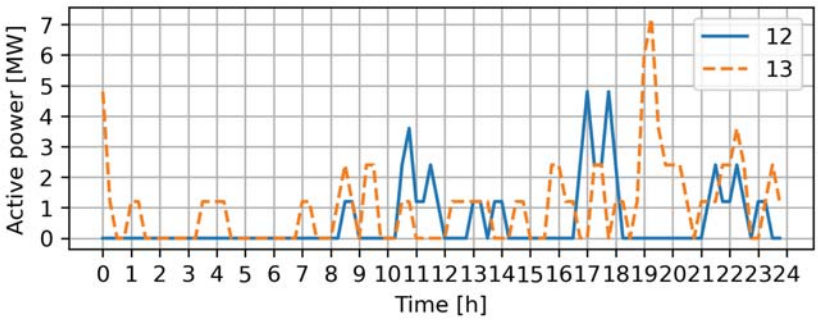

(b) HDEVs are evaluating both the charging price and extra time.

Figure 30: Loading profiles at HPCS 12 and 13 for different evaluation parameters by the HDEVs.

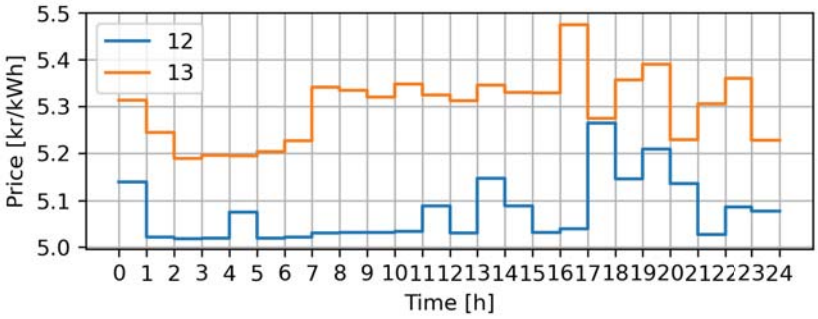

(a) HDEVs are only evaluating the charging price.

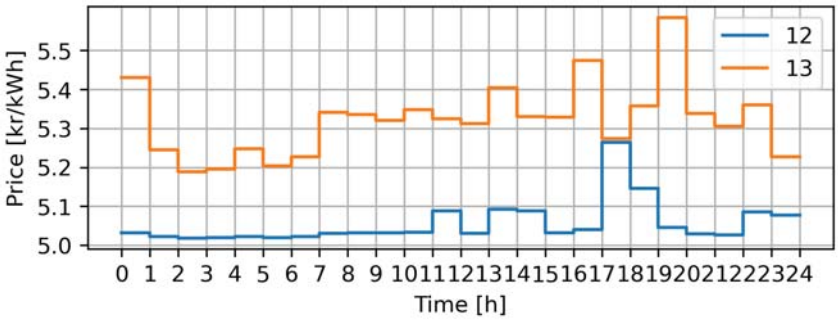

(b) HDEVs are evaluating both the charging price and extra time.

Figure 31: Price profiles at HPCS 12 and 13 for different evaluation parameters by the HDEVs.

7 Discussion

This section aims to discuss the main findings from section 6. Some results were analysed in the previous section. Thus this section will discuss the main findings from the results. Further, will shortcomings and uncertainties in the input parameters be discussed. At last, some considerations on how to implement dynamic pricing in reality and other applications of the model are done.

7.1 Comparing OPF and voltage-based dynamic pricing.

The results from the case studies are showing promising results for both dynamic pricing schemes. It is clear that the dynamic pricing schemes affect the load profiles at the two HPCSs. By investigating two different power system topologies, it is evident that the methods are strongly dependent on the system topology. The performance of OPF dynamic pricing, and especially the voltage-base dynamic pricing, was significantly different at the two topologies.

In the first topology, the OPF based dynamic pricing scheme raised the daily median voltage with 0.001 p.u. at the weakest bus 13, while the reduction in voltage magnitude at bus 12 was marginal. This supports that the pricing scheme is affecting the system conditions favourably. However, the daily minimum voltage magnitudes were reduced at both buses. Again, the change was marginal at bus 12, while it was significantly reduced at bus 13, with some voltage magnitudes to be reduced with 0.03 p.u. It showed that the use of dynamic pricing might mostly improve the voltage quality but at the same time causing the most challenging events to be more challenging. In the second topology, the performance of the OPF based dynamic pricing scheme was better. The unwanted effect of amplifying certain voltage drops was removed, and median voltage magnitudes were further improved.

Applying the voltage-based dynamic pricing scheme at the first topology caused the grid conditions to be worse compared to the fixed pricing scheme. The reason is that most of the load shift appeared from HPCS 12 to HPCS 13, which leads to an increase in the load at the weakest node 13. Both the median voltage magnitude and the minimum voltage magnitude were considerably reduced, while the voltage magnitudes at bus 12 correspondingly increased. In the second topology, the effect of applying the voltage-based dynamic pricing scheme was as desired. It improved the median and minimum voltage magnitude nearly to the same extent as the OPF based dynamic pricing scheme.

Both pricing methods have shown that they can utilise spatial flexibility to improve the voltage quality at the connected buses. In addition to the voltage quality, the amount of energy delivered from the external grid has been impacted. The two pricing schemes have shown for the second investigated topology that spatially moving the loads also may reduce the transmission losses in the system by moving the load to a bus with a better grid connection. It is also clear that the OPF dynamic pricing reduces the losses to a greater extent than the voltage based dynamic pricing. The system losses were 4.57 % and 4.64 %, respectively, for the OPF and Voltage based dynamic pricing, which is a reduction from 4.74 % with fixed pricing. The better results with OPF dynamic pricing may be due to the generated price signals from the OPF are computed from a problem that has its objective to reduce the power injection and thus reducing the system losses.

In general, the OPF based-dynamic pricing scheme has performed better than the voltage-based pricing scheme. One significant difference in the voltage intervals at the voltage-based dynamic

pricing is set manually and must, to a greater extent, be tuned to each system topology independently to create varying prices. This problem is not present with the OPF based dynamic pricing, as the prices a generated based on whichever parameters in the system and not based on an interval for only one parameter. Another important aspect is how the agent-based model has defined the behaviour of the vehicles if the two charging prices are equal. It is reasonable that the drivers are choosing the closest HPCS if the prices are equal. This system turned out unfavourable for the weakest bus 13, as a greater number of vehicles had HPCS 13 as the closest HPCS when the grid condition, in general, was at its most challenging. Due to the possibility of equal prices with the voltage-based dynamic pricing scheme is quite high, this turned out unfavourable for the pricing scheme.

7.2 Better approaches for load data input to the OPF problem

The case studies show that the presented OPF based dynamic pricing strategy and its implementation have some shortcomings and can be improved. As stated earlier, an unwanted phenomenon occurred when the dynamic pricing schemes were applied to the first power system topology. Even though the voltage profiles, in general, become better, it is a chance of amplifying the voltage drops at some time steps, causing the minimum value observed at a simulated day to worsen.

One weakness in how the method is implemented is the input of load data to the OPF problem. When the nodal prices are calculated for the next hour, it is given the load condition of the system in the previous time step. Thus, the nodal price is strongly dependent on a single snapshot. In this snapshot, it can occur load events that do not depict a reasonable load trend for the next hour. This load event may deviate substantially from the rest of the period, causing the nodal prices to be too high or too low. One potential solution to cope with this is to use, e.g., the average load demand in the last hour. This will cause the nodal price to reflect a bigger trend in the load and not only a single event.

Another factor is that an offline approach is used. This approach generates price signals based on how the grid condition was in previous time steps, as stated earlier. It does not make price signals based on predictions on how the grid conditions are in the future. This offline approach does not know that the traffic volume may increase significantly from one hour to the next or how the baseload changes from one time step to the next. Thus, the price may be too low compared to the load demand, causing the price signals to enhance unwanted charging behaviour. An interesting way to continue the work on the dynamic pricing scheme would be to develop a methodology that can price the HPCS based on future grid conditions.

By using historical measurements of the general load in the system, the DSO already knows an expected load pattern for future time steps. Thus, it should be possible to calculate nodal prices that will correspond to the future load demand based on this measurement data directly or by introducing machine learning to predict a future load pattern. However, it would not be completely accurate as the actual system conditions always deviate from historical data or predicted scenarios. Thus, the calculated prices based on the data can be a basis for the charging prices at the HPCSs. These may then be corrected by using real-time measured load quantities to reflect the actual condition. By combining the real-time measurements and the historical data, it should be possible to generate more accurate prices and do not introduce unwanted events such as price drops when they should have been increased. This real-time correction could be from a new OPF calculation or by using monitored voltage magnitudes as the voltage-based dynamic scheme does.

7.3 Uncertainties in the input parameters

It is important to emphasise that the results in this thesis are based on input parameters that are not precisely equivalent to the real-world parameters. It has been made assumptions in both the behaviour of the agents and the topology of the power system. The power system topology and the associated load profiles are not a precise representation of the real world. A limitation of the study is not to include reactive power. Thus, the baseload and the generated load profiles only consider active power, making the system easier to simulate. However, it creates a well-functioning system to showcase some impacts on the grid different pricing schemes introduce.

It is room for improvement regarding the modelling of the behaviour of the HDEVs. Due to limited data on HDEVs properties and behaviour, it has been taken some freedom when setting the initial SOC and the SOC level before a vehicle approaches an HPCS. The sizes on the parameters were chosen to create a reasonable yet challenging scenario for the power system to manage was done to make it easier to highlight the different effects of applying the dynamic pricing schemes. E.g., it was used a uniform distribution between 0.2 and 0.8. for the initial SOC. A normal distribution may be a more viable option. In addition, the same parameters for the distribution were used for every hour in the simulation. Most likely will there be a pattern in the expected SOC at different times of the day. A different study should investigate how these parameters should be sized to make the tuning for creating different scenarios more intuitive.

The simulation model has incorporated a simple method for the charging power characteristics. The charging power is kept fixed through the whole charging session, while in reality, the charging power will decrease when the SOC is getting closer to its maximum. This would have affected the results as the load demand in the later parts of each charging session would be reduced in terms of magnitude, while the charging sessions would have lasted longer due to the reduced charging power.

7.4 Challenges to implementing dynamic pricing in reality.

Some economic difficulties are encountering when applying this pricing scheme to the real world. The objective of the OPF problem for the dynamic pricing scheme is to minimise generator costs, resulting in reducing transmission losses. Therefore, the generated price signals are used to improve the grid conditions and thus improve the economic and social welfare since less energy is lost. This is very desirable from the perspective of the DSO. However, an improvement in social welfare may, in many cases, compromise the HPCS operator desire for economic profit. It could be challenging to demand an HPCS operator to set an unfavourable price at HPCS due to a more loaded location without any compensation. By strictly following the dynamic pricing scheme, the operator may experience severe financial losses. In a further development of the method of calculating the price signals, it would be useful to make an optimisation problem that also protects the HPCS operators from severe financial losses. This way, it is possible to ensure better operating conditions for the grid and maintain the HPCS operators' economic safety.

Another essential aspect to consider, if applying dynamic pricing in the real world, is that the prices must be predictable and easy to understand. If the prices change too quickly and too much in value, the customers may experience the dynamic pricing too complex and challenging to follow. In this thesis, real-time pricing has been applied in both dynamic pricing schemes. The

OPF based pricing scheme updates the price every hour, while the voltage-based pricing scheme updated the price every 15 minutes. There is a chance that real-time pricing will update the prices too often and be difficult to follow. Thus, a more viable option could be to use a Time-of-use pricing program where the prices are updated less often by dividing the day into different levels of high-peak and off-peak hours that are static for a longer period. Thus, making the charging prices more predictable.

7.5 Applying the model to a more complex system.

The case studies have investigated a system where the HPCSs are connected to the same substation. By using the dynamic pricing strategy proposed in this thesis, it was able to reduce the voltage drops during a day. However, the energy demand from the substation has been marginally reduced. By calculating nodal prices at only one limited area, as in this thesis, the use of spatial flexibility is limited and will primarily improve the voltage quality. The proposed pricing strategy and the utilised model are created to be easily scaled to be used on a more extensive system. Thus, it will be possible to investigate other scenarios, such as the impact of load shifting between HPCS in areas connected to different substations. In those scenarios, it could be possible to improve the operating conditions to the substations, lower the system losses and improve the voltage quality at the buses. However, this approach demands a greater set of data, but it can showcase another way to utilise spatial flexibility in the power grid and HPCSs located in different areas.

8 Conclusion

This study has shown that dynamic pricing can move loads between HPCS to utilise flexibility in the power grid. An agent-based model has been used to investigate the impact of dynamic pricing. The model simulates traffic in an environment where the prices at the HPCS are changed dynamically. This model has been extended to include HDEVs in addition to EVs. A proposed methodology for generating dynamic prices have been presented in this thesis and implemented in the agent-based model. The proposed method calculates an OPF every hour based on the grid conditions to generate nodal prices that reflects the grid conditions and the system losses. The generated nodal prices are then scaled to set a realistic charging price at the HPCSs. In addition, an already implemented dynamic pricing scheme that sets the charging price based on the voltage magnitude at the associated bus is compared with the OPF based dynamic pricing and a fixed pricing scheme.

Case studies in Alvdal have been performed on two different power system topologies. The results have shown that the dynamic pricing schemes can shift load between the two HPCS. The load shift has further caused better grid conditions in terms of better voltage quality and decreased system losses. In topology 2, the daily minimum voltage magnitudes at the weakest bus have, on average, been raised with 0.005 p.u. and 0.004 p.u. with OPF and voltage based dynamic pricing, respectively. While it in certain time steps have increased with 0.02 p.u. for both pricing schemes. The voltage-based dynamic pricing scheme has decreased the losses from 4.75 % to 4.65 %, while the OPF based pricing scheme has reduced the losses further to 4.55 %. The results have shown a positive impact from both dynamic pricing scheme, where the OPF based tend to outperform the voltage based dynamic pricing scheme.

In topology 1, the OPF based dynamic pricing increased the average voltage magnitude at the weakest bus and reduced the system losses marginally. However, the daily minimum voltages were decreased by up to 0.03 p.u. In the same topology, the voltage-based pricing scheme caused the load to primarily be moved from the strong bus to the weak bus. This resulted in the daily minimum voltage magnitudes were decreased by 0.06 p.u. These amplified voltage drops occurred due to shortcomings in how the dynamic pricing schemes are implemented. Both methods are approaches that utilise previously measured load conditions and do not predict the upcoming loads. Thus, the method is poorly adapted to handle significant load changes in the next time steps. This leads to the charging price set at an HPCS may not reflect the upcoming grid conditions when the price is applicable. Thus, the prices may be set unfavourable and causing a more considerable traffic volume to the most loaded HPCS. Thus, it is important to customise the dynamic pricing schemes to the specific power system topology and traffic environment to cause desirable load shifts that will improve the grid conditions.

In the case studies, an additional method of evaluating which HPCS is the cheapest was also demonstrated. It considered a cost related to the extra time and energy used when choosing an HPCS that causes a detour to the destination. The results showed that the number of charging events at the cheapest HPCS was reduced. Further investigations on how this evaluation method contributes to a more realistic behaviour must be conducted.

9 Further work

Some suggestions for further work on the topic are listed below to improve the proposed methodology and the used model.

- Include predictions of the load demand in future time steps to generate more precise price signals. The chance of amplifying unwanted behaviour may be reduced.
- Expand the optimisation problem to ensure economic safety for the HPCS operators, not only considering social welfare and better operating conditions for the DSO.
- Develop an intuitive method of tuning pricing schemes to a given power system topology and traffic environment.
- Include reactive power when modelling the power system and the load from HPCS. Thus, creating more realistic grid conditions.
- Improve the Create a better method of generating driving behaviour.
- Do a sensitivity analysis of the new evaluation method to better tune the dynamic pricing schemes.
- Include a more precise method for the initial SOC level and include more complex charging power characteristics that consider the SOC level.
- Apply the model and methodology on a bigger area containing multiple substations to investigate the impact on substations, bus voltages, and system losses.

References

[1] IEA, 'Global EV Outlook 2020', Tech. Rep., 2020.

[2] Tesla, *Semi — Tesla*, 2020. [Online]. Available: https://www.tesla.com/semi.

[3] Daimler, *Electrified on the highway - Freightliner eCascadia and eM2*. [Online]. Available: https://www.daimler.com/sustainability/climate/ecascadia.html.

[4] IEA, 'Trucks and Buses', IEA, Paris, Tech. Rep., 2020. [Online]. Available: https://www.iea.org/reports/trucks-and-buses.

[5] EU, *Reducing CO2 emissions from heavy-duty vehicles*, 2019. [Online]. Available: ec.europa.eu/clima/policies/transport/vehicles/heavy_en.

[6] *Volvo FL Electric — Volvo Trucks*. [Online]. Available: https://www.volvotrucks.co.uk/en-gb/trucks/trucks/volvo-fl/volvo-fl-electric.html.

[7] *eM2® — Freightliner Trucks*. [Online]. Available: https://freightliner.com/trucks/em2/.

[8] T. Earl, L. Mathieu, S. Cornelis, S. Kenny, C. C. Ambel and J. Nix, 'Analysis of long haul battery electric trucks in EU Marketplace and technology, economic, environmental, and policy perspectives. European Federation for Transport and Environment (T&E)', Tech. Rep., 2018, pp. 17–18. [Online]. Available: https://ec.europa.eu/inea/en/ten-t/ten-t-projects.

[9] SSB, *11823: Registrerte kjøretøy, etter region, drivstofftype, statistikkvariabel og år*, 2020. [Online]. Available: www.ssb.no/statbank/sq/10043891.

[10] SSB, *Bilparken*, 2020. [Online]. Available: www.ssb.no/statbank/sq/10043893.

[11] EMOSS, *EMOSS company presentation*, 2016. [Online]. Available: https://www.zero.no/wp-content/uploads/2016/09/EMOSS-company-presentation-2016-new-.pdf.

[12] L. Fridstrøm, 'Framskriving av kjøretøyparken', TØI, Tech. Rep., 2019.

[13] L.-E. Kalland, *Tilgjengelige og kommende fossilfrie lastebiler - ZERO*, 2020. [Online]. Available: https://zero.no/tilgjengelige-og-kommende-fossilfrie-lastebiler/.

[14] *Elon Musk bekrefter: Tesla Semi settes i storproduksjon — Lastebil.no*. [Online]. Available: https://lastebil.no/Aktuelt/Nyhetsarkiv/2020/Elon-Musk-bekrefter-Tesla-Semi-settes-i-storproduksjon.

[15] IRENA, *INNOVATION OUTLOOK SMART CHARGING FOR ELECTRIC VEHICLES About IRENA*. 2019, ISBN: 978-92-9260-124-9. [Online]. Available: www.irena.org.

[16] C. H. Skotland, E. Eggum and D. Spilde, 'Hva betyr elbiler for strømnettet?', Tech. Rep., 2016.

[17] C. H. Skotland and Ø. F. Høivik, 'Har strømnettet kapasitet til elektriske biler, busser og ferger?', Tech. Rep., 2017. [Online]. Available: www.nve.no.

[18] P. Haugneland, *Ladestasjoner i Norge — Norsk elbilforening*, 2020. [Online]. Available: https://elbil.no/her-finner-du-hurtigladestasjonene-i-norge/.

[19] J. S. Vardakas, N. Zorba and C. V. Verikoukis, 'A Survey on Demand Response Programs in Smart Grids: Pricing Methods and Optimization Algorithms', *IEEE Communications Surveys and Tutorials*, vol. 17, no. 1, pp. 152–178, Jan. 2015, ISSN: 1553877X. DOI: 10.1109/COMST.2014.2341586.

[20] R. Deng, Z. Yang, M. Y. Chow and J. Chen, 'A survey on demand response in smart grids: Mathematical models and approaches', *IEEE Transactions on Industrial Informatics*, vol. 11, no. 3, pp. 570–582, Jun. 2015, ISSN: 15513203. DOI: 10.1109/TII.2015.2414719.

[21] S. Limmer, 'Dynamic Pricing for Electric Vehicle Charging—A Literature Review', *Energies*, vol. 12, no. 18, p. 3574, Sep. 2019, ISSN: 1996-1073. DOI: 10.3390/en12183574. [Online]. Available: https://www.mdpi.com/1996-1073/12/18/3574.

[22] K. Chaudhari, N. K. Kandasamy, A. Krishnan, A. Ukil and H. B. Gooi, 'Agent-based aggregated behavior modeling for electric vehicle charging load', *IEEE Transactions on Industrial Informatics*, vol. 15, no. 2, pp. 856–868, Feb. 2019.

[23] M. Garau and B. N. Torsæter, 'Agent-Based Analysis of Spatial Flexibility in EV Charging Demand at Public Fast Charging Stations', in *IEEE Madrid PowerTech, [To be published]*, 2021.

[24] X. Zhu, B. Mather and P. Mishra, 'Grid impact analysis of heavy-duty electric vehicle charging stations', in *2020 IEEE Power and Energy Society Innovative Smart Grid Technologies Conference, ISGT 2020*, Institute of Electrical and Electronics Engineers Inc., Feb. 2020, ISBN: 9781728131030. DOI: 10.1109/ISGT45199.2020.9087651.

[25] E. Y. Ucer, M. C. Kisacikoglu, F. Erden, A. Meintz and C. Rames, 'Development of a DC Fast Charging Station Model for use with EV Infrastructure Projection Tool', in *2018 IEEE Transportation and Electrification Conference and Expo, ITEC 2018*, Institute of Electrical and Electronics Engineers Inc., Aug. 2018, pp. 934–938, ISBN: 9781538630488. DOI: 10.1109/ITEC.2018.8450158.

[26] J. A. Domínguez-Navarro, R. Dufo-López, J. M. Yusta-Loyo, J. S. Artal-Sevil and J. L. Bernal-Agustín, 'Design of an electric vehicle fast-charging station with integration of renewable energy and storage systems', *International Journal of Electrical Power and Energy Systems*, vol. 105, pp. 46–58, Feb. 2019, ISSN: 01420615. DOI: 10.1016/j.ijepes.2018.08.001.

[27] E. Ivarsøy, B. N. Torsæter and M. Korpås, 'Stochastic Load Modeling of High-Power Electric Vehicle Charging - A Norwegian Case Study', in *SEST 2020 - 3rd International Conference on Smart Energy Systems and Technologies*, 2020, ISBN: 9781728147017.

[28] F. H. Malik and M. Lehtonen, 'Analysis of power network loading due to fast charging of Electric Vehicles on highways', in *10th International Conference - 2016 Electric Power Quality and Supply Reliability, PQ 2016, Proceedings*, Institute of Electrical and Electronics Engineers Inc., Oct. 2016, pp. 101–106, ISBN: 9781509015627. DOI: 10.1109/PQ.2016.7724097.

[29] T. Gnann, S. Funke, N. Jakobsson, P. Plötz, F. Sprei and A. Bennehag, 'Fast charging infrastructure for electric vehicles: Today's situation and future needs', *Transportation Research Part D: Transport and Environment*, vol. 62, pp. 314–329, Jul. 2018, ISSN: 13619209. DOI: 10.1016/j.trd.2018.03.004.

[30] D. Stahleder, D. Reihs, S. Ledinger and F. Lehfuss, 'Impact Assessment of High Power Electric Bus Charging on Urban Distribution Grids', in *IECON 2019 - 45th Annual Conference of the IEEE Industrial Electronics Society*, vol. 1, 2019, pp. 4304–4309. DOI: 10.1109/IECON.2019.8927526.

[31] B. Pea-Da and S. Dechanupaprittha, 'Impact analysis of fast charging to voltage profile in PEA distribution system by Monte Carlo simulation', Institute of Electrical and Electronics Engineers Inc., 2015, pp. 204–208, ISBN: 9781467378635. DOI: 10.1109/ICITEED.2015.7408942.

[32] Y. H. Febriwijaya, A. Purwadi, A. Rizqiawan and N. Heryana, 'A study on the impacts of DC Fast Charging Stations on power distribution system', in *Proceedings of 2014 International Conference on Electrical Engineering and Computer Science, ICEECS 2014*, Institute of Electrical and Electronics Engineers Inc., Feb. 2014, pp. 136–140, ISBN: 9781479984770. DOI: 10.1109/ICEECS.2014.7045233.

[33] K. Yunus, H. De La Parra and M. Reza, *Distribution grid impact of Plug-In Electric Vehicles charging at fast charging stations using stochastic charging model*, 2011. [Online]. Available: https://ieeexplore.ieee.org/document/6020302.

[34] C. Fang, H. Lu, Y. Hong, S. Liu and J. Chang, 'Dynamic Pricing for Electric Vehicle Extreme Fast Charging', *IEEE Transactions on Intelligent Transportation Systems*, vol. 22, no. 1, pp. 531–541, Jan. 2021, ISSN: 15580016. DOI: 10.1109/TITS.2020.2983385.

[35] L. Hou, S. Ma, J. Yan, C. Wang and J. Y. Yu, 'Reinforcement Mechanism Design for Electric Vehicle Demand Response in Microgrid Charging Stations', in *Proceedings of the International Joint Conference on Neural Networks*, Institute of Electrical and Electronics Engineers Inc., Jul. 2020, ISBN: 9781728169262. DOI: 10.1109/IJCNN48605.2020.9207081.

[36] Z. Wei, M. Zhao, W. Liao, S. Cheng and Z. Li, 'Dynamic price optimization strategy for charging power station with electric vehicles', in *2019 4th International Conference on Intelligent Green Building and Smart Grid, IGBSG 2019*, Institute of Electrical and Electronics Engineers Inc., Sep. 2019, pp. 358–361, ISBN: 9781728121482. DOI: 10.1109/IGBSG.2019.8886260.

[37] C. Luo, Y. F. Huang and V. Gupta, 'Dynamic pricing and energy management strategy for EV charging stations under uncertainties', in *VEHITS 2016 - 2nd International Conference on Vehicle Technology and Intelligent Transport Systems, Proceedings*, SciTePress, 2016, pp. 49–59, ISBN: 9789897581854. DOI: 10.5220/0005797100490059.

[38] C. Luo, Y. F. Huang and V. Gupta, 'Stochastic dynamic pricing for EV charging stations with renewable integration and energy storage', *IEEE Transactions on Smart Grid*, vol. 9, no. 2, pp. 1494–1505, 2018, ISSN: 19493053. DOI: 10.1109/TSG.2017.2696493.

[39] Z. Moghaddam, I. Ahmad, D. Habibi and M. A. Masoum, 'A coordinated dynamic pricing model for electric vehicle charging stations', *IEEE Transactions on Transportation Electrification*, vol. 5, no. 1, pp. 226–238, Mar. 2019, ISSN: 23327782. DOI: 10.1109/TTE.2019.2897087.

[40] A. Turpen, *California to get utility-owned EV charging stations with dynamic pricing*, Jan. 2016. [Online]. Available: https://newatlas.com/california-electric-car-utility-charging/41585/.

[41] J. Hildermeier, C. Kolokathis, J. Rosenow, M. Hogan, C. Wiese and A. Jahn, 'Smart ev charging: A global review of promising practices', *World Electric Vehicle Journal*, vol. 10, no. 4, Dec. 2019, ISSN: 20326653. DOI: 10.3390/wevj10040080.

[42] H. Saadat, *Power system analysis*, 3rd. PSA Publishing, 2010.

[43] L. Thurner, A. Scheidler, F. Schäfer, J. Menke, J. Dollichon, F. Meier, S. Meinecke and M. Braun, 'pandapower — An Open-Source Python Tool for Convenient Modeling, Analysis, and Optimization of Electric Power Systems', *IEEE Transactions on Power Systems*, vol. 33, no. 6, pp. 6510–6521, Nov. 2018, ISSN: 0885-8950. DOI: 10.1109/TPWRS.2018.2829021.

[44] J. L. Carpentier, 'OPTIMAL POWER FLOWS: USES, METHODS AND DEVELOPMENTS.', in *IFAC Proceedings Volumes*, vol. 18, Pergamon Press (IFAC Proceedings Series n 3), Jul. 1986, pp. 11–21, ISBN: 0080325432. DOI: 10.1016/s1474-6670(17)60410-5.

[45] R. D. Zimmerman, C. E. Murillo-Sánchez and R. J. Thomas, 'MATPOWER: Steady-state operations, planning, and analysis tools for power systems research and education', *IEEE Transactions on Power Systems*, vol. 26, no. 1, pp. 12–19, Feb. 2011, ISSN: 08858950. DOI: 10.1109/TPWRS.2010.2051168.

[46] I. Wangensteen, *Power System Economics - the Nordic Electricity Market*, 2nd. Fagbokforlaget Vigmostad & Bjørke AS, 2012, ISBN: 978-82-519-2863-2.

[47] E. Bonabeau, 'Agent-based modeling: Methods and techniques for simulating human systems', *Proceedings of the National Academy of Sciences*, vol. 99, no. suppl 3, p. 7280, May 2002. DOI: 10.1073/pnas.082080899. [Online]. Available: http://www.pnas.org/content/99/suppl_3/7280.abstract.

[48] R. Laubenbacher, A. S. Jarrah, H. Mortveit and S. S. Ravi, 'A mathematical formalism for agent-based modeling', Dec. 2007. [Online]. Available: http://arxiv.org/abs/0801.0249.

[49] K. Berg, O. A. Hjelkrem and B. N. Torsæter, 'A proposed methodology for modelling the combined load of electric roads and households for long-term grid planning', in *International Conference on the European Energy Market, EEM*, 2020, ISBN: 9781728169194.

[50] A. H. Halse, H. Samstad, M. Killi, S. Flügel and F. Ramjerdi, 'Verdsetting av framføringstid og pålitelighet i godstransport', Transportøkonomisk institutt, Tech. Rep., 2010.

[51] Fjordkraft, *Ladekart*, 2020. [Online]. Available: https://www.ladestasjoner.no/kart/.

[52] Statens Vegvesen, *Trafikkdata*, 2020. [Online]. Available: https://www.vegvesen.no/trafikkdata/.

[53] NVE, *NVE Atlas*, 2020. [Online]. Available: atlas.nve.no.

[54] Kartverket, *Norgeskart*. [Online]. Available: https://www.norgeskart.no.

Appendix

A Loads and line parameters

Table 9: Overview of units in each end-user group.

Load	**Household**	**Agriculture**	**Industry**	**Shop**	**School**	**Health**
P1	140	13	1	1	0	0
P2	204	19	5	3	1	0
P3	47	14	0	0	0	0
P4	47	4	0	0	0	0
P5	71	27	1	0	0	0
P6	63	12	1	0	0	0
P7	320	6	5	11	3	0
P8	49	10	3	0	0	4

Table 10: Line parameters for topology 1.

From	**To**	**Distance [km]**	**Resistance** $[\Omega/km]$	**Reactance** $[\Omega/km]$	**Max loading [kA]**	**std_type**
1	2	0.300	0.8342	0.382	0.17	34-AL1/6-ST1A 20.0
2	3	0.700	0.8342	0.382	0.17	34-AL1/6-ST1A 20.0
2	4	1.850	0.8342	0.382	0.17	34-AL1/6-ST1A 20.0
1	5	0.310	0.4132	0.36	0.29	70-AL1/11-ST1A 20.0
5	6	0.760	0.8342	0.382	0.17	34-AL1/6-ST1A 20.0
5	7	1.460	0.4132	0.36	0.29	70-AL1/11-ST1A 20.0
7	8	4.340	0.4132	0.36	0.29	70-AL1/11-ST1A 20.0
1	9	1.700	0.2376	0.344	0.41	122-AL1/20-ST1A 20.0
9	10	3.300	0.2376	0.344	0.41	122-AL1/20-ST1A 20.0
10	11	2.400	0.8342	0.382	0.17	34-AL1/6-ST1A 20.0
1	12	1.800	0.4132	0.36	0.29	70-AL1/11-ST1A 20.0
8	13	1.400	0.4132	0.36	0.29	70-AL1/11-ST1A 20.0

Table 11: Line parameters for topology 2.

From	**To**	**Distance [km]**	**Resistance** $[\Omega/km]$	**Reactance** $[\Omega/km]$	**Max loading [kA]**	**std_type**
1	2	0.300	0.8342	0.382	0.17	34-AL1/6-ST1A 20.0
2	3	0.700	0.8342	0.382	0.17	34-AL1/6-ST1A 20.0
2	4	1.850	0.8342	0.382	0.17	34-AL1/6-ST1A 20.0
1	5	0.310	0.4132	0.36	0.29	70-AL1/11-ST1A 20.0
5	6	0.760	0.8342	0.382	0.17	34-AL1/6-ST1A 20.0
5	7	1.460	0.4132	0.36	0.29	70-AL1/11-ST1A 20.0
7	8	4.340	0.8342	0.382	0.17	34-AL1/6-ST1A 20.0
1	9	1.700	0.2376	0.344	0.41	122-AL1/20-ST1A 20.0
9	10	3.300	0.2376	0.344	0.41	122-AL1/20-ST1A 20.0
10	13	1.600	0.4132	0.36	0.29	70-AL1/11-ST1A 20.0
7	12	1.300	0.4132	0.36	0.29	70-AL1/11-ST1A 20.0
13	11	1.500	0.8342	0.382	0.17	34-AL1/6-ST1A 20.0

Table 12: Line parameters for topology 2 in case 4.

From	**To**	**Distance [km]**	**Resistance** $[\Omega/km]$	**Reactance** $[\Omega/km]$	**Max loading [kA]**	**std_type**
1	2	0.300	0.8342	0.382	0.17	34-AL1/6-ST1A 20.0
2	3	0.700	0.8342	0.382	0.17	34-AL1/6-ST1A 20.0
2	4	1.850	0.8342	0.382	0.17	34-AL1/6-ST1A 20.0
1	5	0.310	0.4132	0.36	0.29	70-AL1/11-ST1A 20.0
5	6	0.760	0.8342	0.382	0.17	34-AL1/6-ST1A 20.0
5	7	1.460	0.4132	0.36	0.29	70-AL1/11-ST1A 20.0
7	8	4.340	0.8342	0.382	0.17	34-AL1/6-ST1A 20.0
1	9	1.700	0.2376	0.344	0.41	122-AL1/20-ST1A 20.0
9	10	3.300	0.2376	0.344	0.41	122-AL1/20-ST1A 20.0
10	13	1.600	0.4132	0.36	0.29	70-AL1/11-ST1A 20.0
7	12	5.000	0.4132	0.36	0.29	70-AL1/11-ST1A 20.0
13	11	1.500	0.8342	0.382	0.17	34-AL1/6-ST1A 20.0

B Paper: Heavy-duty electric vehicle charging profile generation method for grid impact analysis

The paper is found on the following pages.

Heavy-duty electric vehicle charging profile generation method for grid impact analysis

Kyrre Kirkbakk Fjær
Dept. of Electric Power Eng.
NTNU
Trondheim, Norway
kyrrekf@stud.ntnu.no

Venkatachalam Lakshmanan
Dept. of Energy Systems
SINTEF Energy Research
Trondheim, Norway
venkat@sintef.no

Bendik Nybakk Torsæter
Dept. of Energy Systems
SINTEF Energy Research
Trondheim, Norway
bendik.torsater@sintef.no

Magnus Korpås
Dept. of Electric Power Eng.
NTNU
Trondheim, Norway
magnus.korpas@ntnu.no

***Abstract*—The transport sector is responsible for 20 % of the global CO_2 emissions. By transitioning from internal-combustion engine to battery-electric vehicles, there is a big potential in reducing the emissions. The upcoming heavy-duty electric vehicles (HDEVs) are expected to have a charging power between 100-1600 kW. A transition to HDEVs can cause challenges to the power grid to deliver the charging power needed. In this paper, a methodology to model the load profile of a high-power charging station for HDEVs is proposed. Generated load profiles with different future shares of HDEVs are used to study the impact on the power grid in a representative area in Norway. The loading of the regional substation exceeds its rated capacity when the share of HDEV is 25%, and its thermal limit when the share is increased to 50%. Extending the mandatory breaks for the drivers, and a corresponding reduction of the charging power, shows promising results.**

***Index Terms*—Electric vehicles, High-power charging, Load modelling, Demand profile, Grid planning, Heavy-Duty Vehicles**

I. Introduction

To cope with the 2° Celsius limit in the Paris agreement, new energy technologies must be included. The transport sector is responsible for 20 % of the CO_2 emissions worldwide. Road transport is the most significant contributor, with 75 % of the emissions from the sector. The second highest contributor to emissions in the road transport segment is road freight. It is accounting for 29.4 % of the total emissions in the transport sector. Half of this share is from heavy-duty vehicles (HDVs) [1]. By changing from classical internal combustion engines (ICE) to fuel-cell or battery-electric vehicles (BEVs), there is a significant potential in reducing the emissions.

An introduction of heavy-duty electric vehicles (HDEVs) will create a demand for new charging infrastructure in addition to the infrastructure meant for other types of electric vehicles (EVs), such as electric cars. The upcoming HDEVs are expected to have batteries in the size of 200-1000 kWh and a charging power ranging between 100-1600 kW [2], [3]. Thus, a transition to HDEVs can cause significant challenges to the power grid to deliver the charging power needed. In this paper, a methodology for generating aggregated load profiles for high-power charging stations (HPCS) for HDEVs is presented. The generated load profiles is then used to investigate the future grid impact on a power grid in a representative area along a highway in Norway.

A. Relevant literature

1) Load modelling: There have been conducted few studies on load modelling of high-power charging stations for HDEVs. However, the main principles are the same for load modelling of HPCS for electric cars. Two different methods are mainly used in literature to build the load model. An agent-based approach is used in [4], where each agent is operating autonomously according to one or several given objectives. Charging specifications, mobility pattern and vehicle type are defined for each agent. In [3], an agent-based model, which is originally developed for electric cars in [5], is used to generate load profiles for HDEVs, by changing the input parameters. A second and more common method is to build the model on stochastic parameters without the autonomous decision-making and interactions between the agents. References [6] and [7] are using Poisson processes with a predefined arrival rate or historical traffic flow data directly. The initial state of charge (SOC) is drawn from various probability distributions in [6]–[8]. In [9], SOC is not used as a parameter. Instead, data from HPCSs in Norway and Sweden containing charging duration is used. Monte Carlo simulations are often applied to evaluate the uncertainty of the stochastic parameters [3], [6], [7].

2) Grid impact: The authors in [3] have performed an analysis of the grid impact of HPCS for HDEVs. To look at vehicles with high enough charging power and battery capacity, HDEVs were defined as vehicles with a driving range of 400-800 km in a single charge. The investigated system had a HPCS with five charging points, à 1.2 MW, integrated. Time series analysis was used to investigate the grid impact. The analysis was conducted with the HPCS placed on different locations based on how suitable the connection point was. At the nodal location where there is sufficient capacity, the voltage never dropped below 0.95 p.u. At the nodal location where there is no sufficient capacity, the voltage dropped below 0.8 p.u.

Other literature focuses mainly on the impact of integrating charging of light-duty EVs or HDEVs with shorter driving range, such as urban electric buses. In [10], the impact of electric buses has been analysed. The mobility model is based on a bus network in Vienna, Austria. During operational hours,

buses are charged for a few seconds at every station or for several minutes at the end-stations of a bus line. The charging power is ranging between 300 and 600 kW. The results implied that most European cities should be capable of integrating lines with electrical buses.

In [11]–[13], the impact from charging EVs with a peak demand ranging from 0.7 to 2.5 MW is investigated. The main finding is that the voltages at times suffer from flickering. However, the voltage drop rarely causes any severe problem. In [12], a load profile with a peak demand of 2.2 MW is applied on a 34-node test feeder. The voltage deviation in the worst-case scenario is observed to be 6 %. The load profile implemented in [13] has a peak demand of 2.5 MW. Initially, the highest loading of the transformer is 80 %. After the addition of an EV HPCS, the maximum loading is raised to 90 %. The voltage at the weakest point in the power grid dropped from 0.95 to 0.93 p.u.

B. Contributions

The main contributions this paper presents are:

- A methodology for generating aggregated load for an HPCS for HDEVs.
- Creation of charging profiles for a real traffic flow using the proposed methodology.
- Grid impact analysis on a power grid inspired by a real power grid topology.

C. Outline

This paper is divided into five sections. Following the introduction in Section I, Section II presents the methodology for generating load profiles for HDEVs and a description of power grid model development. In Section III the investigated system and cases are described. The results from the simulations are presented and discussed in Section IV. Section V concludes and presents the main findings from the research conducted in this paper.

II. Methodology

A. Load profiles for heavy-duty electric vehicles

To generate load profiles for an HPCS for HDEVs, a method for modelling the aggregated load of the HPCS is developed. The proposed method is based on the work performed in [7] which uses a stochastic approach for passenger EVs. Due to less known specifications of HDEVs and their behaviour compared to state-of-the-art electric cars, some simplifications have been made.

1) Simplifications: An unlimited amount of charging points is assumed at the HPCS. Thus, this model does not take vehicle queuing into account. This is done to highlight the possible total power demand in an area, i.e., the worst-case scenario that the network operator must be prepared for. Every heavy-duty vehicle (HDV) driver needs to have a mandatory break of 45 minutes after every 4.5 hours of driving time [14]. Thus, a charging duration is lasting until the battery is fully charged or when the break is over. In this paper, HDEVs are defined as electric trucks with a battery size in the range of 475-1000 kWh and a driving range of 400-800 km in a single charge.

2) Generating traffic flow: The arrival time for each HDEV is decided by using a Poisson process. It is assumed that each HDEV is independent of each other and that the expected number of HDEVs is kept constant in each hour as per the given traffic flow data. However, the expected number of HDEVs entering the system each hour varies throughout the day. Thus, a new Poisson process is conducted for each hour of the day, with different expected values.

Due to no information about the arrival rate of HDEVs, the expected value λ_h for each hour, h, is calculated from the real traffic flow q_h of HDVs and the desired $HDEV share$, (1).

$$\lambda_h = HDEV\ share * q_h \tag{1}$$

The time between each HDEV arriving the HPCS, in minutes, is calculated with (2) as described in [7], where u is a variable that is uniformly distributed between 0 and 1.

$$w = -\frac{60}{\lambda_h} * ln(1-u) \tag{2}$$

The arrival time of the n^{th} vehicle is given by (3).

$$t_n = t_{n-1} + w \tag{3}$$

When the arrival time t_n is greater than or equal to 60 minutes, the Poisson process is finished, and a new process is started with the expected value for the next hour.

3) Generating HDEV objects: After the arrival time for each HDEV has been decided, the HDEVs profile will be created by applying their parameters to generate charging demand profile. Each HDEV is assigned parameter values based on the selected model type. The HDEV model type is drawn from a cumulative distribution function where the probability for choosing each model is equal. The input parameters are battery size, charging power and the probability of selecting a specific HDEV model.

When the HDEV is generated, it is given the initial SOC level when it arrives the HPCS, as $SOC_{arrival}$. The SOC value is drawn from a normal distribution with a standard deviation [15] equal to 0.1. The expected SOC value $\mu_{arrival}$ is decided by the battery size of the HDEV and the average energy used to travel to the HPCS, (4).

$$\mu_{arrival} = 1 - \frac{E_{travel}}{E_{battery}} \tag{4}$$

It is assumed that every HDEV starts the trip fully charged. The battery size, $E_{battery}$, is given for each model. The general energy demand for travelling to the HPCS, E_{travel}, is set by using SINTEF's energy module [16]. The energy module estimates how much energy different vehicle types use for a specific driving route in Norway.

4) Charging: The amount of delivered energy to the HDEV in each time step, $E_{charged,t}$ is found by using (5), where P is the charging power (W) and Δt is the length of the time step. In this paper, the time resolution is one minute. Thus, the charging must be scaled from hours to minutes.

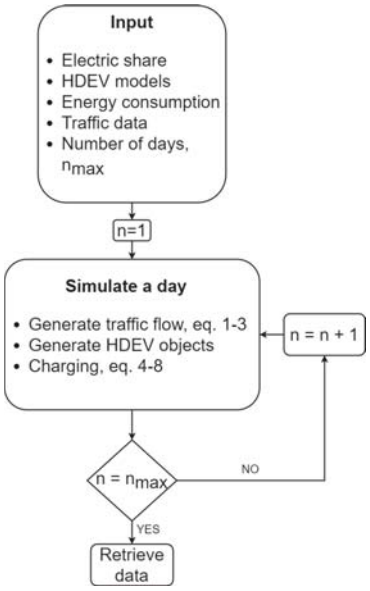

Fig. 1. Flow chart of the proposed method for generating aggregated load for an HPCS for HDEVs.

$$E_{charged,t} = P\Delta t * \frac{1}{60} \tag{5}$$

The maximum SOC level is in this paper set to 95 %, thus the maximum charged energy, E_{max}, is found from (6).

$$E_{max} = (0.95 - SOC_{arrival}) * E_{battery} \tag{6}$$

The HDEV will either charge until the charging session has lasted as long as the mandatory break, T_{break}, (7) or when the maximum charged energy is reached (8).

$$t = T_{break} \tag{7}$$

$$E_{charged} = E_{max} \tag{8}$$

Due to the stochastic parameters, the day is simulated 1001 times to get a representative set of the load profiles. Each load profile is then sorted by the mean energy demand for a time step to find the median load profile. It is chosen to run 1001 simulations to easily find the median profile in the set. A flow chart of the method is presented in Fig. 1.

B. Grid model

A representative power grid is created to observe the impact of HDEV charging. The power grid is created using the open-source package 'pandapower' in Python to conduct AC power flow analysis using the Newton-Raphson method [17]. The grid representation is created by assembling 'pandapower' objects. By using the built-in Timeseries module in 'pandapower', it is possible to iterate through time steps. Thus, load profiles generated from the proposed load modelling method can be applied. The loads in the power grid are divided into two different types, base load and HPCS loads. The base load

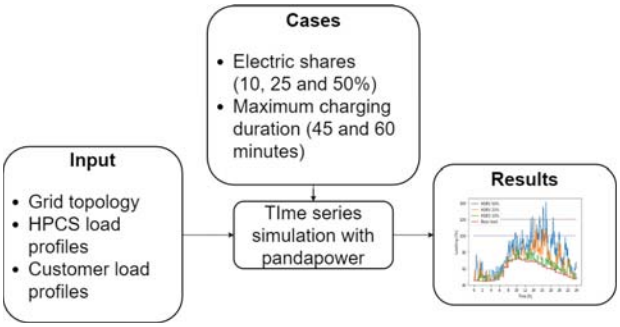

Fig. 2. Overview of the case study.

is created by dividing the surroundings into zones with each node having the aggregated load from the existing customers within that zone. The aggregated loads are made by combining demands from e.g., households, farms and schools, using general profiles created in the earlier research by SINTEF Energy Research [18]. In addition, HPCS loads for electric cars and HDEVs are included. The load profiles for electric cars that charges from HPCS are made by using the method presented in [7], while the HDEV charging demand is made using the method presented in this paper.

III. Case study

A real-life case study has been conducted on a small village in Eastern Norway, where 90 % of all HDVs driving between Oslo and Trondheim are passing by. The selected location is an established and designated lay-by area for HDVs, and refreshment point for drivers. The substation has its highest loading during the winter, thus the simulations are based on winter conditions to challenge the power system the most.

In this paper, the grid impact due to two different parameters, namely electric share and maximum charging duration, have been investigated. Simulations with three different electric shares, (10 %, 25 % and 50 %), of HDVs are conducted to observe the effect on the grid with potential electric shares in the future. The introduction of HDEVs may introduce high demand peaks. To reduce the demand peaks a possible charging strategy is applied. By extending the mandatory break from 45 to 60 minutes it is possible to reduce the charging power and still deliver the energy needed for charging the vehicle. An overview of the grid impact study for the different cases are presented in Fig. 2.

A. Traffic flow

The traffic flow is based on historical data recorded by the The Norwegian Public Roads Administration [19]. The traffic data is filtered to only include vehicles with a length greater than 12.5 meters. The traffic flow passing by the HPCS is presented in Fig. 3.

B. State of charge

In addition to arrival time, the SOC of the visiting HDEV has a great impact on the load profile of the HPCS. It is assumed that all HDEVs are starting at Oslo or Trondheim.

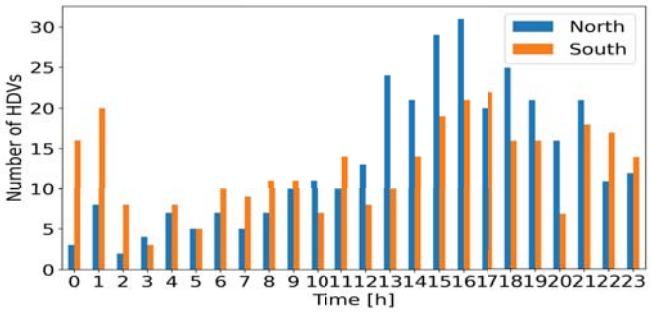

Fig. 3. Hourly measured traffic flow of HDVs, divided in driving directions north and south.

TABLE I
DISTANCE, ENERGY AND DRIVING EFFICIENCY USED BETWEEN THE STARTING POINT AND THE HPCS.

Starting point	Distance [km]	Energy [kWh]	Driving efficiency [kWh/km]
Oslo	291	414	1.42
Trondheim	172	256	1.49

The energy demand from driving to the HPCS from Oslo and Trondheim is found in Table I. The proposed driving efficiency of the Tesla is 1.25 kWh/km [20], which is slightly lower than the generated values from the energy module. Due to the winter conditions that are assumed in this model, the driving efficiency will likely be worse than the proposed values from Tesla. Thus, the values from the energy module are used as an expected value for the energy demand.

C. HDEV models

To the best of the authors knowledge, there is no HDEVs operating at this route today. To make a representative HDEV fleet, the upcoming Tesla Semi and Freightliner eCascadia are considered. Both models are long haul vehicles with an expected driving range of at least 400 km in a single charge. The Tesla Semi is also chosen as they already have received orders from Norway. In addition, the two HDEV models showcase two different scales of future HDEVs. Tesla Semi has a battery size and charging power over double the size of the Freightliner eCascadia. In table II the input parameters for each model are presented. The charging power of the Tesla Semi is scaled down from 1.6 MW to 1.333 MW to appreciate the charging power variations during the charging session.

D. Power system topology

The grid model is based on a grid topology located in the county called Innlandet in Eastern Norway. It contains 13 buses that are connected to the regional grid via a 66/22 kV substation transformer. Bus 0-10 is the existing topology and the aggregated customer loads. Bus 11 and 12 represent two HPCS, one for electric cars and one for HDEVs. It is assumed that both are connected directly to the transformer. The single-line diagram is presented in Fig. 4.

TABLE II
INPUT PARAMETERS FOR THE HDEVS TO THE LOAD MODEL

HDEV model	Battery size [kWh]	Charging power [kW]
Tesla Semi	1000	1333
Freightliner eCascadia	475	400

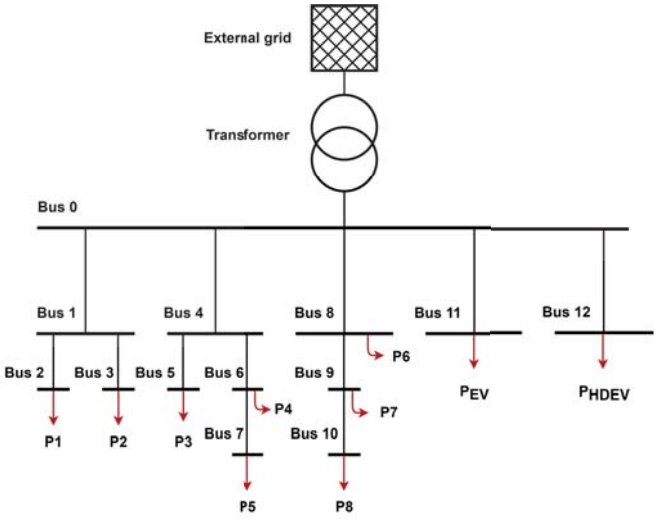

Fig. 4. Single line diagram for the grid model.

At the located area there are several HPCSs. To model the load profile, these HPCSs are combined and modelled as a single HPCS with 20 charging points. Sixteen outlets having a capacity of 150 kW and four with 350 kW. The representation of the EV fleet is made by choosing the ten most registered EV models in Norway [21]. The load profile for the HPCS for HDEVs is created with parameters as described in Section III.

IV. RESULTS AND DISCUSSION

A. Load profiles

The generated load profiles, with a one-minute time resolution, in Fig. 5 shows that charging of HDEVs introduces demands with major changes in the load demand. They represent the median profile of each case. When the electric share is 10 %, the demand is evenly distributed through the day and the peaks are rarely above 4 MW. In the cases where the electric share is increased to 25 % and 50 % there are greater variations in the load. The peak demand are mainly around 9 MW and 13 MW respectively. These peaks are quite high compared to HPCS for electric cars. To generate peaks in the sizes of 13 MW it is needed 85 outlets à 150 kW operating at full capacity. Thus, the load impact from HDEVs is significant compared to EVs. It is important to note that the method used in this paper assumes that all charging demand is served. This is done to observe a worst-case day for the DSO. The results are thus potentially overestimating the demand in some cases.

One potential way to reduce the peaks is to extend the mandatory breaks for the drivers, which allows lowering

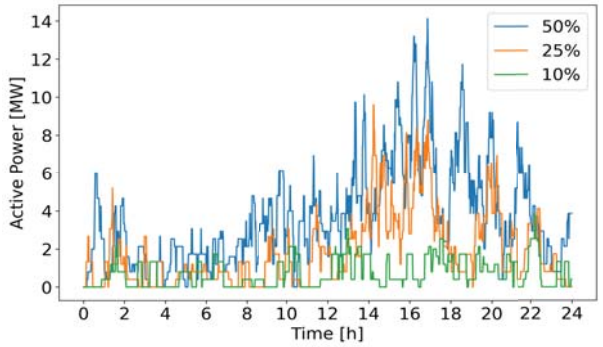

Fig. 5. The resulting median load profiles from the simulations with electric shares of 10 %, 25 % and 50 %.

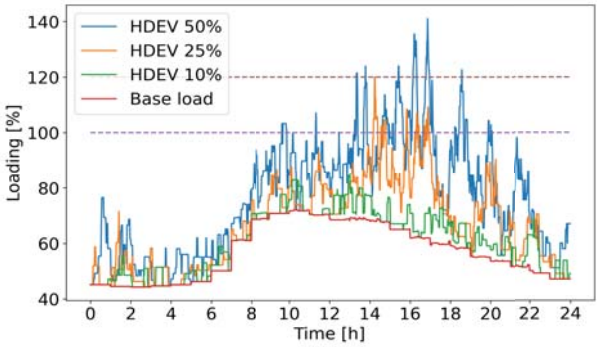

Fig. 7. Transformer loading for the base load and HPCS loads with electric shares of 10 %, 25 % and 50 %.

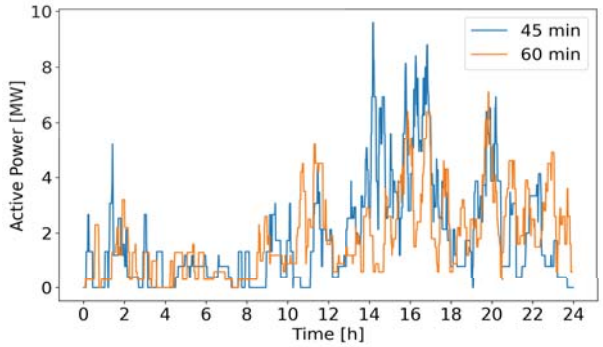

Fig. 6. The resulting median load profiles from the simulations with 25 % electric share. Shown with both 45 and 60 minutes mandatory break.

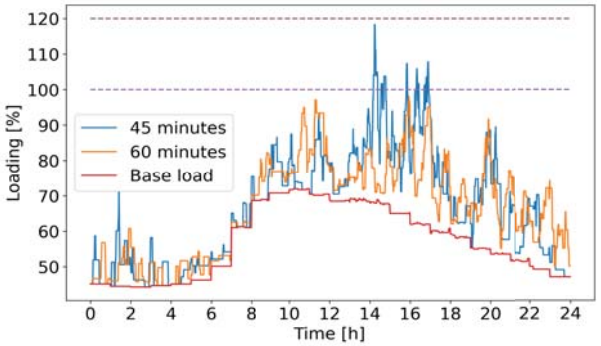

Fig. 8. Transformer loading for the base load and HPCS load with electric share of 25 %. Shown with both 45 and 60 minutes mandatory break.

the charging power. The resulting median load profiles for the ”25 % case” are presented in Fig. 6. By extending the maximum charging duration from 45 to 60 minutes, the highest peaks were reduced with approximately 2 MW. Consequently, the load demand throughout the day has less difference in the values at the peaks and valleys, which causes a more predictable load.

B. Grid impact

The generated load profiles were further used in power flow analysis to investigate the impact on the local substation transformer and the voltage quality. From the simulations, it is evident that the loading from the HDEV HPCS makes a significant impact on the transformer loading, presented Fig. 7. In the ”25% case”, the rated capacity is exceeded in certain time steps in the interval between 14 and 17. The exceeding peaks never reach the theoretical thermal limit at 120 %, which allows the transformer to still operate as long it is for short periods only. When the electric share is further increased to 50 %, the overloading increase both in time and magnitude, causing the transformer to exceed its thermal limit.

To minimise the operating time with overload in the ”25 % case”, the load profiles with extended charging duration were applied. By extending the charging duration to 60 minutes, the operating time with overload is removed, seen in Fig. 8. It is still possible to experience overload as the presented results are using the median profile.

The majority of the base load is connected to bus 9 and 10 and is the buses with the lowest voltages. Fig. 9 presents the voltages when there is only the base load in the system, and when the electric share of HDVs is 25 % and 50 %. It is evident that the introduction of HDEVs causes great fluctuations in the voltages. In the ”25 % case”, the largest voltage drop occurs around 14, when the voltages decrease with 0.01 p.u. The number of events when the voltage decreases with at least 0.01 has increased in the ”50 % case”. At 17, the voltage drops approximately 0.02 p.u.

V. Conclusion and Further Work

This paper has presented a methodology for modelling the aggregated load profile of an HPCS used by HDEVs. In the study, it is assumed that all the load demand from HDEVs is served to show a worst-case day for the DSO. The generated load profiles were further used in a grid impact study of a representative area in Eastern Norway. The HPCS introduced a significant load to the system with peak values equal to 4 MW, 9 MW and 13 MW for three different HDEV shares, respectively (10 %, 25 % and 50 %). These loads caused the associated substation to exceed the rated capacity when the HDEV share was 25 % and exceed the thermal limit when the share was further increased to 50 %. A proposed strategy of

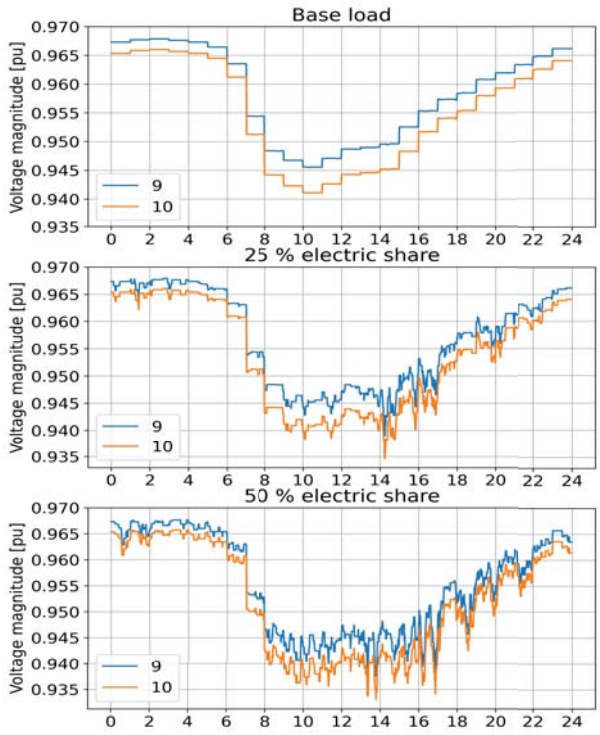

Fig. 9. Voltages at bus 9 and 10 with base load and different electric shares.

extending the drivers' mandatory breaks from 45 to 60 minutes and lower the charging power correspondingly to maintain the same energy demand were applied. This resulted in a reduction in the peak load of the HPCS, and the substation to operate below rated capacity. The methodology may overestimate the load demand. Thus, a verification of the methodology will be conducted when validation data is available. This approach is fully dependent on the input parameters and a sensitivity analysis of the input parameters to discover potential errors in the generating data due to inaccuracies in the input should be investigated. To highlight a more realistic behaviour of the HDEVs, queuing will be implemented in the method in further work.

Acknowledgment

The authors gratefully acknowledge the Research Council of Norway and industry partners for the support in writing this paper under project 295133/E20 FuChar - Grid and Charging Infrastructure of the Future. The authors would also like to thank Elvia, a Norwegian DSO, for their contribution of grid data for this study.

References

[1] IEA, "Trucks and Buses," IEA, Paris, Tech. Rep., 2020. [Online]. Available: https://www.iea.org/reports/trucks-and-buses.

[2] IEA, "Global EV Outlook 2020," Tech. Rep., 2020.

[3] X. Zhu, B. Mather, and P. Mishra, "Grid impact analysis of heavy-duty electric vehicle charging stations," in *2020 IEEE Power and Energy Society Innovative Smart Grid Technologies Conference, ISGT 2020*, Institute of Electrical and Electronics Engineers Inc., Feb. 2020, ISBN: 9781728131030.

[4] K. Chaudhari, N. K. Kandasamy, A. Krishnan, A. Ukil, and H. B. Gooi, "Agent-based aggregated behavior modeling for electric vehicle charging load," *IEEE Transactions on Industrial Informatics*, vol. 15, no. 2, pp. 856–868, Feb. 2019.

[5] E. Y. Ucer, M. C. Kisacikoglu, F. Erden, A. Meintz, and C. Rames, "Development of a DC Fast Charging Station Model for use with EV Infrastructure Projection Tool," in *2018 IEEE Transportation and Electrification Conference and Expo, ITEC 2018*, Institute of Electrical and Electronics Engineers Inc., Aug. 2018, pp. 934–938, ISBN: 9781538630488.

[6] J. A. Domínguez-Navarro, R. Dufo-López, J. M. Yusta-Loyo, J. S. Artal-Sevil, and J. L. Bernal-Agustín, "Design of an electric vehicle fast-charging station with integration of renewable energy and storage systems," *International Journal of Electrical Power and Energy Systems*, vol. 105, pp. 46–58, Feb. 2019, ISSN: 01420615.

[7] E. Ivarsøy, B. N. Torsæter, and M. Korpås, *Stochastic Load Modeling of High-Power Electric Vehicle Charging-A Norwegian Case Study*. 2020, ISBN: 9781728147017.

[8] F. H. Malik and M. Lehtonen, "Analysis of power network loading due to fast charging of Electric Vehicles on highways," in *10th International Conference - 2016 Electric Power Quality and Supply Reliability, PQ 2016, Proceedings*, Institute of Electrical and Electronics Engineers Inc., Oct. 2016, pp. 101–106, ISBN: 9781509015627.

[9] T. Gnann, S. Funke, N. Jakobsson, P. Plötz, F. Sprei, and A. Bennehag, "Fast charging infrastructure for electric vehicles: Today's situation and future needs," *Transportation Research Part D: Transport and Environment*, vol. 62, pp. 314–329, Jul. 2018, ISSN: 13619209.

[10] D. Stahleder, D. Reihs, S. Ledinger, and F. Lehfuss, "Impact Assessment of High Power Electric Bus Charging on Urban Distribution Grids," in *IECON 2019 - 45th Annual Conference of the IEEE Industrial Electronics Society*, vol. 1, 2019, pp. 4304–4309.

[11] B. Pea-Da and S. Dechanupaprittha, "Impact analysis of fast charging to voltage profile in PEA distribution system by Monte Carlo simulation," Institute of Electrical and Electronics Engineers Inc., 2015, pp. 204–208, ISBN: 9781467378635.

[12] Y. H. Febriwijaya, A. Purwadi, A. Rizqiawan, and N. Heryana, "A study on the impacts of DC Fast Charging Stations on power distribution system," in *Proceedings of 2014 International Conference on Electrical Engineering and Computer Science, ICEECS 2014*, Institute of Electrical and Electronics Engineers Inc., Feb. 2014, pp. 136–140, ISBN: 9781479984770.

[13] K. Yunus, H. De La Parra, and M. Reza, *Distribution grid impact of Plug-In Electric Vehicles charging at fast charging stations using stochastic charging model*, 2011. [Online]. Available: https://ieeexplore.ieee.org/document/6020302.

[14] Statens vegvesen, *Kjøre- og hviletid — Statens vegvesen*, 2020. [Online]. Available: https://www.vegvesen.no/kjoretoy/yrkestransport/kjore-og-hviletid/kjore-og-hviletid.

[15] H. Liang, Z. Lee, and G. Li, "A Calculation Model of Charge and Discharge Capacity of Electric Vehicle Cluster Based on Trip Chain," *IEEE Access*, vol. 8, pp. 142 026–142 042, 2020, ISSN: 21693536.

[16] O. A. Hjelkrem, P. Arnesen, H. Karlsson, E. Dahl, O. Kåre Malmin, and O. M. Rennemo, "Planning for a system wide electrification of the transport sector in Norway," in *32nd Electric Vehicle Symposium (EVS32) Lyon, France, May 19 - 22, 2019*, Lyon, 2019.

[17] L. Thurner, A. Scheidler, F. Schäfer, J. Menke, J. Dollichon, F. Meier, S. Meinecke, and M. Braun, "pandapower — An Open-Source Python Tool for Convenient Modeling, Analysis, and Optimization of Electric Power Systems," *IEEE Transactions on Power Systems*, vol. 33, no. 6, pp. 6510–6521, Nov. 2018, ISSN: 0885-8950.

[18] K. Berg, O. A. Hjelkrem, and B. N. Torsæter, *A proposed methodology for modelling the combined load of electric roads and households for long-term grid planning*, ISBN: 9781728169194.

[19] Statens Vegvesen, *Trafikkdata*, 2020. [Online]. Available: https://www.vegvesen.no/trafikkdata/.

[20] Tesla, *Semi — Tesla*, 2020. [Online]. Available: https://www.tesla.com/semi.

[21] *Registreringer av nye elbiler i Norge*. [Online]. Available: https://elbilstatistikk.no/.

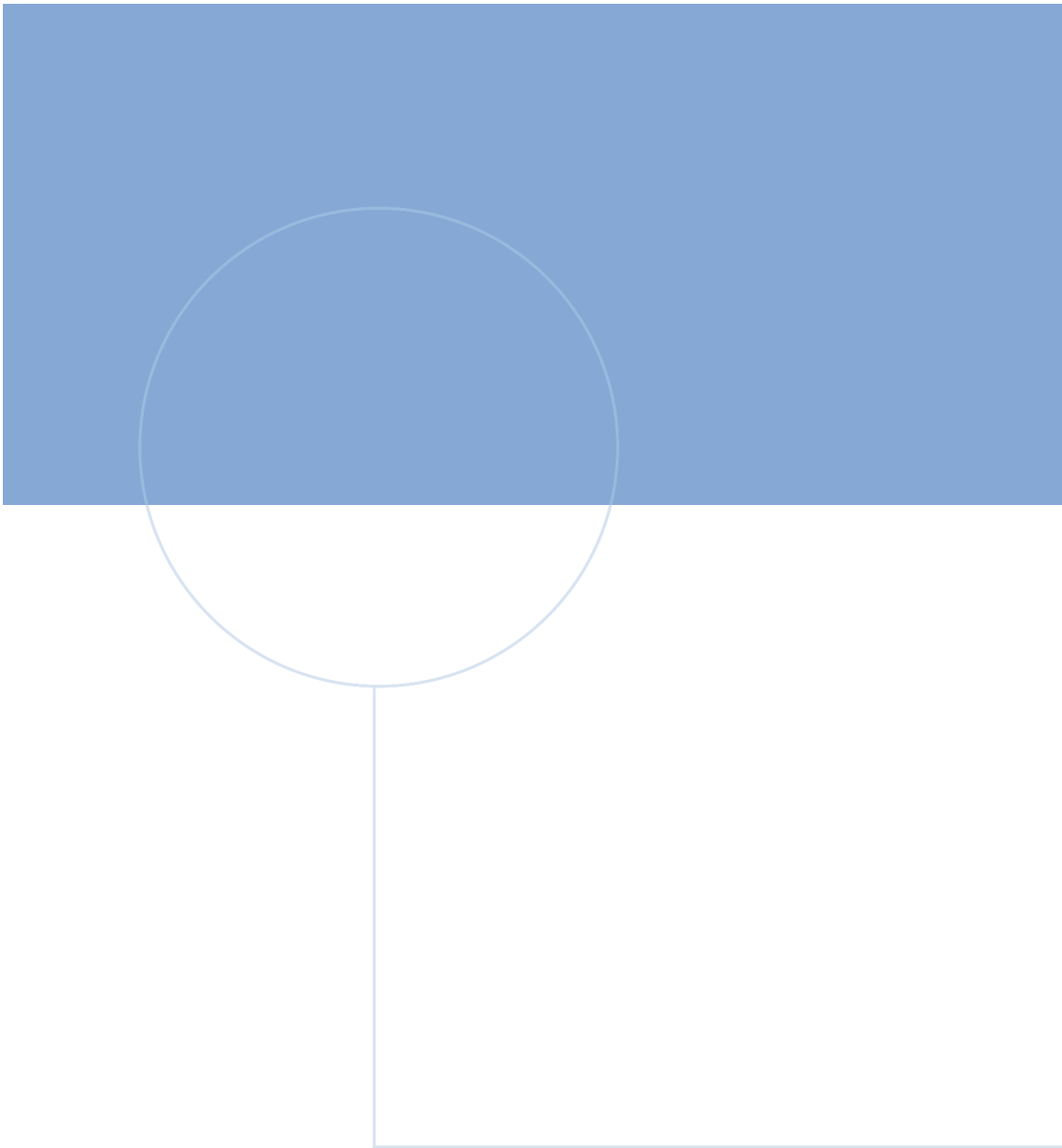

NTNU

Norwegian University of
Science and Technology